UNIVERSIDADE FEDERAL DE PERNAMBUCO
DEPARTAMENTO DE FÍSICA – CCEN
PROGRAMA DE PÓS-GRADUAÇÃO EM FÍSICA

LUCAS DE QUEIROZ DA COSTA CAMPOS

DIPOLAR SELF-PROPELLED MATTER: DYNAMICAL STRUCTURES AND APPLICATIONS IN TRANSPORT OF PASSIVE MATTER

Recife
2016

LUCAS DE QUEIROZ DA COSTA CAMPOS

DIPOLAR SELF-PROPELLED MATTER: DYNAMICAL STRUCTURES AND APPLICATIONS IN TRANSPORT OF PASSIVE MATTER

Dissertação apresentada ao Programa de Pós-Graduação em Física da Universidade Federal de Pernambuco, como requisito parcial para a obtenção do título de Mestre em Física.

Orientador:
Prof. Dr. Sérgio Wlademir da Silva Apolinário

Recife
2016

Catalogação na fonte
Bibliotecária Joana D'Arc Leão Salvador CRB 4-572

C198d Campos, Lucas de Queiroz da Costa.
Dipolar self-propelled matter: dynamical structures and applications in transport of passive matter / Lucas de Queiroz da Costa Campos. – 2016.
64 f.: fig., tab.

Orientador: Sérgio Wlademir da Silva Apolinário.
Dissertação (Mestrado) – Universidade Federal de Pernambuco. CCEN. Física, Recife, 2016.
Inclui referências.

1. Matéria condensada. 2. Matéria ativa. 3. Partículas Janus. 4. Colóides dipolares. I. Apolinário, Sérgio Wlademir da Silva (Orientador). II. Titulo.

530.41 CDD (22. ed.) UFPE-FQ 2017-02

LUCAS DE QUEIROZ DA COSTA CAMPOS

DIPOLAR SELF-PROPELLED MATTER: DYNAMICAL STRUCTURES AND APPLICATIONS IN TRANSPORT OF PASSIVE MATTER.

Dissertação apresentada ao Programa de Pós-Graduação em Física da Universidade Federal de Pernambuco, como requisito parcial para a obtenção do título de Mestre em Física.

Aprovada em: 16/12/2016.

BANCA EXAMINADORA

_____

Prof. Dr. Sérgio Wlademir da Silva Apolinário
Orientador
Universidade Federal de Pernambuco

_____

Prof. Dr. Marcelo Andrade de Filgueiras Gomes
Examinador Interno
Universidade Federal de Pernambuco

_____

Profª Drª Kaline Rabelo Coutinho
Examinadora Externa
Universidade de São Paulo

À minha mãe, por me mostrar que em tudo existe beleza.
Só temos que procurar.
Ao meu pai, por me mostrar que em tudo existe sentido.
Só temos que entender.

A Fátima Bahia e a Paula Almeida, por sempre arranjarem
tempo e disposição para responder as dúvidas de um
jovem Lucas sobre os mistérios do universo.

Acknowledgements

This work was supported by the Brazilian Science Agency, CNPq, and developed in collaboration with Profs. F. M. Peeters, F. Q. Potiguar and Prof. W. P. Ferreira.

Resumo

Nesta dissertação, nós investigamos partículas dipolares auto-propulsoras, suas propriedades dinâmicas e sua capacidade de transportar matéria passiva. Nós utilizamos Dinâmia Browniana, através da equação de Langevin, para modelar a interação entre as partículas e o solvente. Inicialmente nós simulamos o sistema para vários conjuntos de parâmetros e mapeamos os diversos valores dos momentos de dipolo e campo externo às estruturas formadas pelas partículas magnéticas. Analisamos então como estas estruturas poderiam ser utilizadas no transporte de matéria passiva. Nós descobrimos que no regime diluído, a causa mais proeminente de transporte era a colisão direta entre as partículas passivas e ativas, resultando em uma grande diferença entre a velocidade média quadrática entre os dois tipos de partícula. Em casos densos, nós observamos uma cristalização em sistemas com momento de dipolo pequeno, enquanto partículas com alto momento de dipolo podiam formar veias no cristal, e até se separar em regiões distintas. Nós também estudamos matéria ativa cuja direção do momento de dipolo era ortogonal à direção de auto-propulsão. Nós observamos o surgimento de um novo mecanismo de transporte, no qual a partículas ativas envolvem e varrem as partículas passivas. Esta provou ser a forma mais eficiente de transporte de matéria passiva em regimes dilutos, resultando em velocidade médias quadráticas até seis vezes maiores que aquelas obtidas quando a direção do momento de dipolo e a direção da auto-propulsão eram paralelos.

Palavras-chave: Matéria Frágil. Matéria Ativa. Partículas Auto-Propulsoras. Partículas Janus. Colóides Dipolares.

Abstract

In this MSc. Thesis we investigate the dynamical properties of dipole-like self-propelled particles and their abilities to transport otherwise passive matter. We use Brownian Dynamics, via the Langevin equation, to model the interaction between the particles and the solvent. First, we simulated various sets of parameters, mapping the resulting structures formed by the magnetic active particles for several values of dipole moment and external field. Then, we analysed how these structures could aid in the transport of passive particles. We found that in dilute regimes, the preeminent cause of transport was the head-on collisions between active and passive particles, resulting in a large gap in the mean squared velocity of the two kinds of matter. In dense systems, we observed a freezing of the active-passive ensemble in systems with a low dipole moment, while particles with high dipolar moment could form veins in the crystal, and even separate into distinct regions. We also studied the magnetic active matter whose magnetic moment direction was orthogonal to that of its self-propulsion. We observed a new mechanism of transport arise, where the active particles would envelope and sweep the passive particles. This proved to be the most efficient method of transport of passive matter by self-propelled particles in dilute regimes, resulting in mean squared velocities six times larger than those obtained for parallel active particles.

Keywords: Soft Condensed Matter. Active Matter. Self-Propelled Particles. Janus Particles. Dipole-like Colloids.

List of Figures

Contents

1 Introduction

É pequenina é miudinha é quase nada
mas não tem outra mais bonita no lugar.
—LUIZ GONZAGA (Boiadeiro)

In this work, we will study the dynamics of dipole-like active colloids. In order to make sense of the barrage of keywords in the previous sentence, this section aims to provide a bird's-eye view on several topics, starting with our fundamental blocks, colloids, in Subsec. 1.1. The idea of Brownian motion will be introduced in Subsec. 1.2. Then, in Subsec. 1.3 we will present some uses and fabrication methods of dipole-like colloids, followed by an overview of active matter in Subsec. 1.4.

1.1 Colloids

Colloids are ubiquitous in the modern world. Their adoption ranges from high-tech industry, where they are used for instance in imaging, oil recovery, and liquid crystals; to the everyday household life, where they can be found in the milk we drink and the paint which colours our houses (HIEMENZ, 1997).

Despite being used since at least the 5th century BCE (ANGELINI et al., 2004; ARTIOLI; ANGELINI; POLLA, 2008)[1], only in 1833 were there efforts to define colloids precisely[2]. The first of those definitions was conducted by Thomas Graham (GRAHAM, 1833). He studied the diffusion of liquids through a membrane and called the solutions that did not diffuse *colloidal solutions.*[3]

Modern definitions do not look at diffusive properties of the solution, but rather prefer to take properties inherent to the particles – rather than those of the membrane – to characterize the material. However, defining colloids in a way that encompasses all the instances where the

[1] Some sources also mention the usage of aerosol in Ayurvedic medicine over 4000 years ago (GANDEVIA, 1974; GROSSMAN, 1994).

[2] For a review on the usage of colloids throughout history, see (SCIAU, 2012)

[3] The term colloid derives from the Greek word *kola*, which means glue (ISLAM, 2016).

term is currently used is a difficult task. Some, like (HAMLEY, 2008) and (HIEMENZ, 1997) use the size of the particles as the defining criteria. Indeed, they define colloids as particles whose dimensions range from 1nm to 1 μm. This definition is accepted by the International Union of Pure and Applied Chemistry (IUPAC) (JONES et al., 2009), which defines colloids as

> 2.6 colloid
> A short synonym for a colloidal system.
> 2.7 colloidal
> State of subdivision, implying that the molecules or polymolecular particles dispersed in a medium have at least in one direction a dimension roughly between 1 nm and 1 μm, or that in a system discontinuities are found at distances of that order.

A more functional approach is to define colloids as particles that are small enough that they have a non-negligible interaction with their solvent, but large enough that this interaction is only present in a statistical sense. As summarised by (DHONT, 1996), "they are large, but not too large".

1.2 Brownian Dynamics

In most real life applications colloids are immersed in a solvent. As is known since the early 19th century, colloidal particles immersed in a liquid will exhibit an erratic movement (DHONT, 1996). The credit for the discovery of this random motion is often given to the botanist Robert Brown. In 1827 he was studying the motion of granular pollen suspended in water under a microscope. He observed that the pollen exhibited irregular motion, such as the one presented in Fig.1.1. However, the phenomenon had already been reported by Ingen-Housz (INGEN-HOUSZ; MOLITOR, 1784) in 1784.

At first, Brown assumed the motion was related to the living properties of the pollen particles. However, when the experiment was redone with inorganic matter, the jittery movement was still present, removing the possibility of the source of the motion being life-related (BROWN, 1828).

The origin of this motion remained a mystery until 1863 when experiments conducted by Wigner, who was well acquaintance with Maxwell's kinetic theory, proved that the cause of this movement is due to the thermal collisions with the molecules in the liquid (WIGNER,

Figure 1.1 Time evolution of a particle in a solvent. This particle experiences an erratic movement typical of Brownian motion.

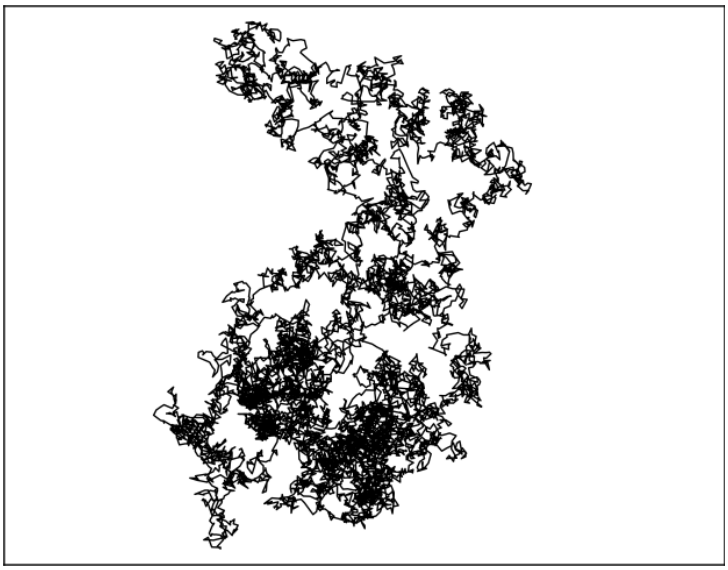

1863). In the 20th century, Einstein (EINSTEIN, 1956), Smoluchowski (SMOLUCHOWSKI, 1906) and Langevin (LANGEVIN, 1906) provided the theoretical framework to show that the behaviour of the Brownian particles were indeed due to the collision between the macroscopic particle and the thermally agitated particles of the solvent. A cabal experiment was conducted by Perrin (PERRIN; ROUEN, 1913), confirming the theoretical findings and determining the Avogrado number. For this work he was awarded the Physics Nobel Prize, in 1926 (AB, 2014).

1.3 Dipole-like Particles

Systems of magnetic particles dispersed in liquids are very interesting to industry due to their combination of fluid and magnetic properties, which can be exploited in various applications, such as biomedical operations (PANKHURST et al., 2003), sealing (CABUIL, 2000), viscous damping (ALVAREZ; KLAPP, 2013) and brakes (SCHERER; NETO, 2005).

There are several ways to synthesize dipolar particles. The simplest way is to build colloids out of ferromagnetic materials, such as nickel (SNEZHKO; ARANSON, 2011)[4]. A refinement of this approach is to envelope a magnetic nucleus with a non-metallic material (PALACCI et al., 2013), which protects the magnetic core from abrasion.

We can also assemble a special kind of colloid, called Janus Particle (JP), with magnetic

[4]These simpler colloids are commercially available <https://www.alfa.com/en/catalog/A17943/>.

Figure 1.2 (a) Nickel(II) colloids obtained by ageing $Ni(NO_3)_2$ in urea. Taken fom (PORTA et al., 1999) (b) A polymer sphere of 3-methacryloxypropyl trimethoxysilane, surrounding most (but not all) of an hematite cube. Taken from (PALACCI et al., 2013) (c) Poly(styrene-block-2-vinylpyridine) spheres covered in OsO_4, forming a Janus Particle. Taken from (YABU et al., 2010).

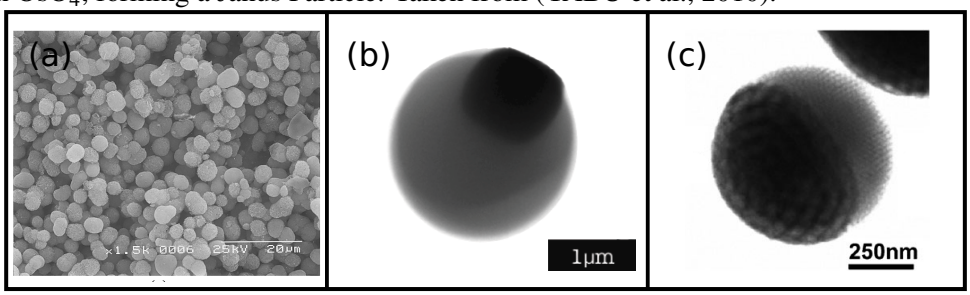

properties. Janus Particles are colloids which lack material uniformity. This asymmetry impart different chemical and physical properties (WALTHER; MÜLLER, 2013). JPs can be produced in a multitude of ways, but producing nanoscopic JPs can still be challenging. The common strategies to prepare nanosopic Janus Particles were derived from organic chemistry, employing self-assembly, protein engineering and polymer synthesis (WALTHER; MÜLLER, 2013). It is possible to assemble magnetic JPs by coating monodisperse colloids with magnetic thin films, endowing the particles with magnetic responsiveness (YAN; BAE; GRANICK, 2015).

It is also possible to induce a dipole moment in polystyrene particles, using an alternate current electric field (VELEV; GANGWAL; PETSEV, 2009). This approach takes advantage of frequency-dependence polarization of the particles. The difference between dielectric permittivity and conductivity of the particle and of the surrounding media will dictate the sign and magnitude of the induced dipole moments (MORGAN; GREEN, 2003).

We can take this idea one step further, and try to induce dipolar interactions on Janus particles using AC fields. In (GANGWAL et al., 2010) polystyrene particles with gold patches covering a sizeable portion of the colloids were used. These particles were immersed into deionized water and confined by two glass plates, creating a quasi-bi dimensional film. However, higher multipole moments were also activated (GANGWAL et al., 2010; SCHMIDLE et al., 2013).

1.4 Active Matter

In the last few years, a novel class of biological and physical systems, referred to as active matter, have been a hot topic. These systems are composed of particles, defined by (RAMASWAMY, 2010) as “active particles contain internal degrees of freedom with the ability

to take in and dissipate energy and, in the process, execute systematic movement". The term active matter was first used in (SCHIMANSKY-GEIER et al., 1995) to refer to Brownian particles that generate a field, which, in turn, influenced their motion. Later, other authors used this term to denote self propelled particles far from equilibrium (EBELING; SCHWEITZER; TILCH, 1999; ROMANCZUK et al., 2012). To this day, artificial self propelled particles are one of the focusses of the area (VICSEK et al., 1995; CZIRÓK; STANLEY; VICSEK, 1997). However, it is known that several other systems behave in an active fashion, such as flagellate cells (ROMANCZUK et al., 2008) and groups of macroscopic animals (COUZIN et al., 2005; SUMPTER et al., 2008; GUTTAL; COUZIN, 2010).

Currently, one of the main interests in active matter is understanding how the dynamics of the bulk emerges from the properties of single particles (ELGETI; WINKLER; GOMPPER, 2015). Several papers were written studying solitary particles (BÖDEKER et al., 2010; FRIEDRICH; JÜLICHER, 2007; HOWSE et al., 2007) and larger systems (CHATÉ; GINELLI; MONTAGNE, 2006; BASKARAN; MARCHETTI, 2009; VICSEK et al., 1995).

Another very important feature of most active matter systems are the random fluctuations affecting individual agents. These fluctuations need not be thermal in nature but may come from all kinds of sources. While many indeed arise from thermal action, a good number are caused by internal processes of the agent. One well known example are the internal reorganization of bacteria (PATNAIK, 2012; DRESCHER et al., 2011). Most often, these fluctuations are accounted for without explicitly solving their driving mechanisms. Instead, one can model them by introducing random forces into the equations of motion of the particles. Thus, it is very common to use Langevin and Fokker-Plank equations when dealing with active particles (ROMANCZUK et al., 2012)[5].

[5]Reviews on the theory and recent results in the area can be found in (ROMANCZUK et al., 2012) and (ELGETI; WINKLER; GOMPPER, 2015).

2 Simulation Techniques

Computers are like Old Testament gods; lots of rules and no mercy.

—JOSEPH CAMPBELL (The Power of Myth)

Most of the findings in this work were possible due to the usage of computer simulations. In this section, we intend to give the reader an brief overview on the topic. In Subsection 2.1, we present the history of Molecular Dynamics and lay its theoretical foundations. The Molecular Dynamics Technique is adapted in Subsec. 2.2 to deal with Brownian Dynamics simulations, using the Langevin Equation. In Subsection 2.3 we derive the integration algorithm we will use throughout the remaining sections of this MSc. thesis. We mention ways to simulate ensembles other than the microcanonial one in Subsec 2.4, followed by a brief discussion on numerical stability and the choice of parameters in Subsec. 2.5.

2.1 Molecular Dynamics

The creation of Molecular Dynamics (MD) was a foregone conclusion. Most of the theoretical tools needed to perform MD simulations were created decades, if not centuries, before the first Molecular Dynamics program was implemented. By the 1940's the only component still needed was the digital computer on which the simulations were to run. As such, not many years passed between the availability of computers and the first MD realization.

The first commercial computer, BINAC, was delivered to Northrop in 1949 (STERN, 1979) [1]. In 1957 Alder was already able to calculate statistical properties of systems using MD (ALDER; WAINWRIGHT, 1957). In 1964 Rahman published his computational results on hard sphere systems which agreed with experiments (RAHMAN, 1964) and by 1967 Verlet was doing a methodical study of computer experiments in fluids (VERLET, 1967).

To understand the basics of MD, only a basic knowledge of classical mechanics and differential calculus is required. Namely, Newton's 2nd law in the differential form. In this

[1] However, only a single machine was ever delivered and it never worked properly. The first commercial computer with some widespread usage (in 1950's standards) was the UNIVAC (JOHNSON, 2006).

dissertation we will always work with point-like, chemically inert particles. These are comparetively simple to simulate. However, some more complex mathematics may be required for some other cases. For instance, had we worked with extended objects, Euler equations and quaternions would be better suited for the job.

In Classical Mechanics, the state of three dimensional systems of N particles is fully described by $6N$ quantities, the coordinates $\mathbf{q}^N = (q_1, q_2, \ldots, q_{3N})$ and the momenta $\mathbf{p}^N = (p_1, p_2, \ldots, p_{3N})$ of the particles. Newton's 2nd law can be written in the following manner:

$$\frac{dp_i}{dt} = F_i(\mathbf{q}^N, \mathbf{p}^N) = -\left[\nabla U(\mathbf{q}^N, \mathbf{p}^N)\right]_i, \tag{2.1}$$

where F_i is the total force acting on the coordinate i, U describes the potential energy of the system and the nabla symbol is the gradient operator. Therefore, what distinguishes two different physical systems is their potential energy functions and their boundary conditions. We will go through some examples of both.

2.1.0.1 Potential Energy Examples

Interaction Potentials

Undoubtedly the interparticle potential with the most widespread usage in literature is the Lennard-Jones (LJ) potential. It was first proposed in 1924 by Lennard-Jones, long before MD was ever implemented (JONES, 1924). Such potential was used to model neutral atoms' interaction, incorporating in a simple and successful way both the long-range attractive force due to van der Waals potentials and the short-range repulsion due to proximity of electron clouds. The interaction energy between two particles, i and j, with an interparticle distance r_{ij} given by the following expression:

$$U(r_{ij}) = 4\varepsilon\left[\left(\frac{\sigma}{r_{ij}}\right)^{12} - \left(\frac{\sigma}{r_{ij}}\right)^{6}\right], \tag{2.2}$$

where the parameter ε dictates the depth of the potential well and σ the location of the minimum. Indeed, for any given σ the minimum is located at $r_0 = 2^{1/6}\sigma$.

This potential is largely used to model atomic interactions of systems both in gas (JONES, 1924) and crystals (ASHCROFT; MERMIN, 2011). Note that one of the greatest advantages of the Lennard-Jones potential for MD simulations is its simplicity. Indeed, given the squared distance between particles, r_{ij}^2, it is possible to calculate $U(r_{ij})$ using only five multiplications, one division and a sum. Furthermore, using r_{ij}^2 instead of r_{ij} we can avoid calculating an expensive square root. These simplicities allows one to devote computational time to do larger

Figure 2.1 Graph of the Lennard-Jones potential for the parameters $\sigma = \varepsilon = 1.0$. The minimum of the potential is found at the value $r_{ij} = 2^{1/6} \approx 1.122$.

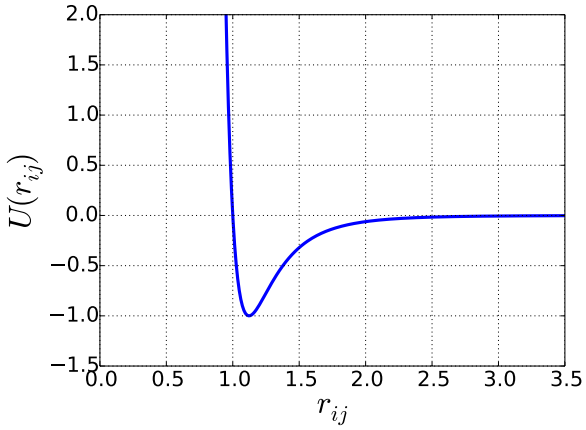

and longer simulations.

Another commonly used potential is the Yukawa potential. It was first published in 1937 as an interaction model for the strong force between nucleons (YUKAWA, 1935). However, it was soon noticed that such potential can be used to model the interaction between charged particles surrounded by an ionized solvent. These particles have an external layer of free ions (DHONT, 1996) which screens the interparticle potential. That means that the potential energy decreases at much faster rate than a simple Coulomb Potential. The Yukawa Potential can be written as

$$U(r_{ij}) = \frac{q^2}{r_{ij}} e^{-\kappa r_{ij}}, \tag{2.3}$$

where κ measures the effectiveness of the screening. As expected, when $\kappa \to 0$ we recover the original Coulomb Potential.

However, care must be taken in this limit. When one uses Periodic Boundary Conditions (which will be explained in detail in Subsec. 2.1.0.2) to simulate an infinite number of particles in a three-dimensional space one must make sure that the energy integral does not diverge. While a naïve sum may yield wrong results, techniques such as Ewald summation can solve this issue (ALLEN; TILDESLEY, 1989).

One can should notice that both of the interaction potentials aforementioned were pair-wise interactions. This is not the only kind of interparticle potential, but it is the most often used. However, some effects only occur when many-body potentials are used. Silicon, for instance, crystallizes into a diamond cubic crystal structure and to fully reproduce this lattice in simulations, a three-body potential is necessary (RAPAPORT, 2004).

Nonetheless, avoiding many-body potentials is very common, as when using these poten-

Figure 2.2 Yukawa potential for a few values of κ, as indicated within figure. The charge was set to unity.

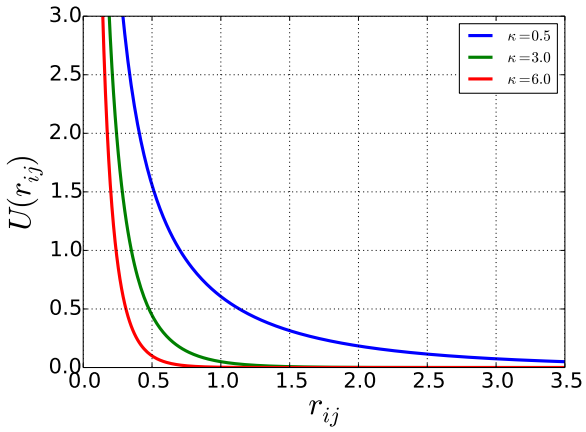

tials the algorithm complexity grows rapidly. For instance, while the calculation of a pairwise potential is $\mathcal{O}(N^2)$ the algorithm to calculate a three body potential will be of class $\mathcal{O}(N^3)$. In general, a D-body potential will require calculations of order $\mathcal{O}(N^D)$.

The Big-O notation used in the last paragraph describes how the number of steps needed to complete calculation scales. For instance, $\mathcal{O}(N^2)$ means that the computational time is expected to grow with the second power of the number of particles. Therefore, doubling the number of particles would increase the simulation time fourfold.

External Potentials

Not only interparticle potentials play a role in MD. Commonly external traps are used to confine colloids (LÖWEN, 2009). Examples of confinements are optical tweezers (CHOWDHURY; ACKERSON; CLARK, 1985) and external electromagnetic fields (ZAHN; MÉNDEZ-ALCARAZ; MARET, 1997; LÖWEN et al., 2005). The simplest way to model either of these is the parabolic external potential.

$$V(r_i) = \kappa r_i^2. \tag{2.4}$$

The gradient of Eq. 2.4 in cartesian coordinates will depend linearly on the coordinates. Thus there is no need to calculate r_i or even r_i^2, avoiding any expensive calculations. Another advantage is that the previous equation is very generic. Any confining potential can be cast in the shape of Eq. 2.4 by a Taylor expansion up to second order. For a generic confining potential $\phi(r_i)$ centered around the origin we can calculate the value of the spring constant as $\kappa = (d^2\phi/dr_i^2)|_{r_i=0}$.

Quantum Effects

As mentioned in the first paragraph of the previous subsection, the theoretical foundations of MD are those of Classical Mechanics, which were laid from the 17th century to late 19th century. Then it should come as no surprise that while MD only flourished in the second part of the 20th century it completely ignored two of its most important theoretical breakthroughs: Quantum Mechanics and Relativity.

Ignoring Relativity poses no big issue to the description of the systems presented in this dissertation. The velocities of atoms in crystals are much smaller than the speed of light and the distances are small enough that within the time discretization, information spreads in sub-luminal speeds and causality is not broken. However, one might rightfully complain that these same small distances force our system to fall well within the Quantum Mechanics (QM) validity region. Moreover, Molecular Dynamics is based upon the idea that is possible to have complete knowledge of the system's positions and momenta at any given instance. This is in grave contrast to QM and its founding principle of uncertainty.

These issues can be partially solved by a wise usage of the freedom of choice in the potential energy function U. For instance, it is possible to follow a semi-classical approach and include effects that, while quantum in nature, can be cast in a classical vesture (MAITLAND et al., 1983). This allows MD to be used in an even broader range of problems. The three-body interactions are common examples of the necessity of this semi-classical approach. Its heart lay in quantum mechanics (RAPAPORT, 2004), but it is possible to create models of potential energies that mimic satisfactorily the real system (STILLINGER; WEBER, 1985).

2.1.0.2 Boundary Conditions

Alone, Eq. 2.1 describes objects in an infinite, homogeneous and boundless space. When dealing with colloidal systems, this is rarely the case as colloids are mostly found in containers of some kind. Consequently, one would expect the simulation to also include boundaries.

Based on the real world, a first idea might be that of hard-wall boundaries. In microscopic terms, this means that a particle which hits the simulation box boundary has its velocity reflected around the normal vector of the wall. That way, one restricts the movement of the particles only to a finite region in space.

However, this is rarely the most efficient condition. In real world systems most of the particles are located in the bulk of the system, rather than at the borders. For a three dimensional system of $N \approx 10^{23}$ particles at liquid density the amount of particles at the border is about $N^{2/3} \approx 10^{15}$. That is, one particle in every 10^8.

By today's standards, a rather large simulation would have N in the order of tens of thou-

sands[2]. We can use the same argument as before to find that the number of particles in the border is $N^{2/3} \approx 10^3$ or one in every ten particles. Therefore, the border effects, which in real world systems matter for a relative tiny amount of particles would be much more noticeable in simulations.

Unless the object of research is the interaction between colloids and containers it would be useful to use a boundary condition that allows us to focus our computational efforts in the bulk of the system rather than at the brink. This can be achieved with periodic boundary conditions (PBC).

The implementation of PBC is rather simple. Whenever a particle reaches the limits of the simulation box it is transported to the opposite side of the box, with its momentum unchanged. A schematic representation of hard-wall conditions and PBC can be seen in Fig. 2.3.

Figure 2.3 A single particle being simulated with hard-wall boundaries (left) and PBC (right). In the left figure the momentum in the x-axis is reflected and in the right figure the momentum is kept constant while the x-coordinate is wrapped.

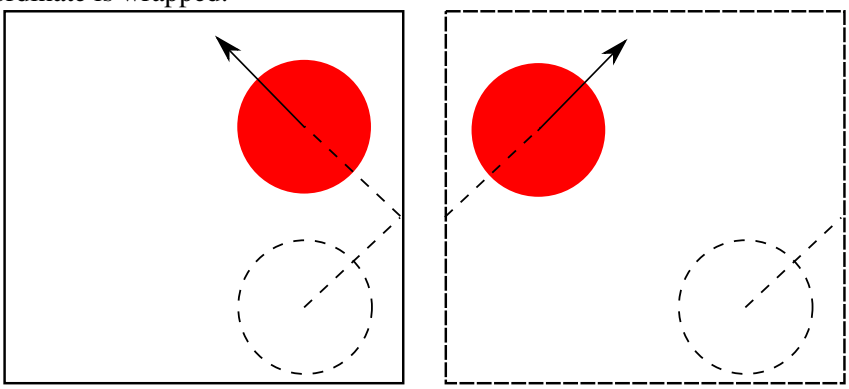

PBC has the advantage that it allows us to understand properties of an infinite system while using only a finite number of particles. Indeed, by using as few as 256 hard-spheres and PBC it is possible to reproduce well known statistical properties, such as the phase diagram and the velocity distribution of the system, as expected by the Statistical Mechanics theory (HAILE, 1992).

2.2 Simulating Brownian Dynamics

As mentioned in Subsec 1.2, colloids are most commonly found in solutions, surrounded by a fluid. A simplistic approach to simulate this system would be to run calculations for both kind

[2]But by no means would that simulation be considered immense. In (WATANABE; SUZUKI; ITO, 2011), for instance, 4,096,000,000 particles interacting via Lennard-Jones potential were simulated.

of particles, the colloids and the molecules of the solvent. This is a terrible idea.

The molecules in the liquid exhibit a relaxation time in the order of 10^{-14}s, while colloidal relaxation times are closer to 10^{-9}s (DHONT, 1996). This difference of five orders of magnitude makes simulating the fluid and the colloids using MD prohibitively expensive. Far too much computational time would be spent simulating the liquid, as the number of such molecules far exceed that of colloids and many more time steps would be needed to see any representative movement of the colloids.

It is much wiser to use a macroscopic approach on this problem and take advantage of the theory developed in the beginning of the last century by Einstein, Smoluchowski and Langevin, as mentioned in Subsec. 1.2. In doing so, we abandon Newton's 2nd Law and use Langevin's equation to describe the system dynamics instead. For a system of N particles with masses m and interaction potential U, the Langevin's equation is (DHONT, 1996)

$$m\frac{d^2r_i}{dt^2} = F(t) - \gamma\frac{dr_i}{dt} + \eta(t), \tag{2.5}$$

where γ is the drag constant and η is a white noise satisfying

$$\langle \eta(t) \rangle = 0, \langle \eta(t)\eta(t') \rangle = 2\gamma k_B T \delta(t-t'), \tag{2.6}$$

where brackets indicate an average over the generalized coordinates $\mathbf{q}^N$ and $\mathbf{p}^N$. Besides the Brownian motion, the liquid also has a viscosity and commonly in experimental setups, the solvent is viscous enough that causes it the colloidal accelerations to be very small. In other words, the system will present an overdamped motion, where $\frac{d^2r_i}{dt^2} \approx 0$. In that way, we can rewrite Langevin's equation as

$$\frac{dr_i}{dt} = \frac{1}{\gamma}\left(F(t) + \eta(t)\right). \tag{2.7}$$

Do notice, however, that this equation has an stochastic term, η, which cannot be dealt by the classical methods to solve ODEs, such as Runge-Kutta (RK), Verlet and Leapfrog. Indeed, a whole new class of algorithms is needed to simulate these equations.

2.3 First Order Stochastic Runge-Kutta

In this subsection we will deduce the first-order member of a family named Stochasic Runge-Kutta (SRK). The classic RK methods can be seen as a special case of these new algorithms and are recovered when the noise is null. In this subsection, we will closely follow the derivation presented in (HONEYCUTT, 1992).

First we will analyse the one-variable, first order stochastic equation,

$$\frac{dx}{dt} = f(t) + g(t). \tag{2.8}$$

This equation has a deterministic part, $f(t)$ and a stochastic part, $g(t)$. The latter is a white-noise gaussian process, with properties

$$\begin{aligned} \langle g(t) \rangle &= 0 \\ \langle g(t)g(t') \rangle &= 2D\delta(t-t'), \end{aligned} \tag{2.9}$$

where D is some constant and $\delta(t)$ is Dirac's delta. We can develop our algorithm in the following manner: first, integrate Eq. 2.9 from $t = 0$ to $t = \delta t$,

$$x(\delta t) = x(0) + \int_0^{\delta t} f(t')dt' + \Gamma(\delta t) \tag{2.10}$$

where $\Gamma(\delta t) = \int_0^{\delta t} g(t')dt'$. Next we suppose that f(t) is constant in the integration time. That is, the resulting algorithm will only be first order. Thus, the last can be rewritten as

$$x(\delta t) = x(0) + f(0)\delta t + \Gamma(\delta t). \tag{2.11}$$

Now, we will deduce the properties of $\Gamma(\delta t)$. First, as $\langle g(t) \rangle = 0$, the average of Γ will also be null. To calculate the variance, one more piece is needed, $\langle \Gamma(t)\Gamma(t') \rangle$.

$$\begin{aligned}
\langle \Gamma(t)\Gamma(t') \rangle &= \int\int \left(\int_0^{t'} g(\tau')d\tau' \int_0^{t''} g(\tau'')d\tau'' \right) d\mathbf{q}^N d\mathbf{p}^N \\
&= \int\int \left(\int_0^{t'} \int_0^{t''} g(\tau')g(\tau'')d\tau''d\tau' \right) d\mathbf{q}^N d\mathbf{p}^N \\
&= \int_0^{t'} \int_0^{t''} \left(\int\int g(\tau')g(\tau'')d\mathbf{q}^N d\mathbf{p}^N \right) d\tau''d\tau' \\
&= \int_0^{t'} \int_0^{t''} \langle g(\tau')g(\tau'') \rangle d\tau''d\tau' \\
&= \int_0^{t'} \int_0^{t''} 2D\delta(\tau'-\tau'')d\tau''d\tau' \\
&= \int_0^{t'} 2Dd\tau' \\
&= 2Dt'
\end{aligned}$$

As stated above, this algorithm is only first order. However, by following a similar scheme one can deduce algorithms of arbitrary order. The interested reader is encouraged to see (HONEYCUTT, 1992) for a detailed discussion on higher-order Stochastic Runge-Kutta.

Now, one can readily make the following identifications: $x \to r_i$, $f \to \frac{1}{\gamma}F$, $g \to \frac{1}{\gamma}\Gamma$ and $D \to \gamma k_B T$. These result in the following algorithm

$$r_i(\delta t) = r_i(0) + \frac{1}{\gamma}F(0)\delta t + H(\delta t), \tag{2.12}$$

where $H(t)$ is a gaussian white noise with properties

$$\begin{aligned}
\langle H(t) \rangle &= 0 \\
\langle H(t)H(t') \rangle &= 2\gamma k_B T \delta t.
\end{aligned} \tag{2.13}$$

That is to say, the stochast term $H(\delta t)$ will be result into a discrete translation in a random direction. This is the final form of the integration scheme we will use in the following sections.

2.4 The Ensembles

The attentive reader might have noticed one fundamental thing changed when we started using Langevin's Equation instead of Newton's 2nd Law. No longer are we simulating a NVE en-

semble[3]. Now, instead of the energy, the temperature is kept constant, which means that we are simulating the NVT ensemble. This does not present an issue here, as most experiments are done in exactly these conditions.

We would like one to notice, however, that Brownian Dynamics is not the only way to simulate the NVT ensemble. Standard MD can be modified in another way: Instead of using Langevin's Equation it is possible to extend the Hamiltonian of the system by adding a virtual "friction"[4] that will be responsible for keeping the temperature constant. This has the advantage of keeping the system well withing the tooling of Classical Mechanics. Indeed, in this fashion it is possible to simulate any other ensemble by adding different constraints for pressure (ANDERSEN, 1980), temperature (NOSÉ, 1984; NOSÉ, 1991) or chemical potential (LYNCH; PETTITT, 1997).

Another method to achieve the non-microcanonical ensemble relies on the addition of stochastic thermostats alongside the hamiltonian equations of motion. This has the disadvantage of any analyses on properties of the algorithm must be done via Markov Chains rather than via Hamiltonian Dynamics (ANDERSEN, 1980).

2.5 Further Considerations and Numerical Stability

Part of the art of Molecular Dynamics is how to find the proper simulation parameters. It is possible to do theoretical analyses of algorithms, but only for very simple systems. For anything more complicated than a few basic examples there is no hard and fast rule on how to set the simulation parameters and its values must be found in a somewhat empirical fashion. Choose an excessively small value of δt, for instance, and the simulations will take a long time to finish, wasting computational time. On the other hand, with a large value of δt errors will accumulate and spurious values will result.

Another unavoidable source of error in computer simulations is the finiteness of the floating point representation used in modern computers. This topic is out of the scope of this work, but a good primer on this subject can be found in (GOLDBERG, 1991).

[3] That is, the number of particles, N, the volume, V, and the temperature, T are kept constant.

[4] The resulting quantity can only be called friction in a very loose sense, as it is possible the value of the friction will be negative, thereby increasing the energy of the system.

3 Dynamical Structures

You are the way and the wayfarers.

—KAHLIL GIBRAN (The Prophet)

In order to understand the transport of passive matter, we first analyse the formations assembled by active particles. We will use the methods layed in the previous section to run computer simulations of active particles in isolation and study their structural possibilites. The knowledge of these structures will pave the way into the actual transport of passive matter, and guide us into the possibilities of transportation.

This section is organized as follows. In Subsection 3.1, we describe the model we used, the simulations details. We specify how the measurements were performed in Subsec. 3.2. In Subsection 3.3, we present the results, for systems in low and high magnetic field regimens. Finally, in Subsection 3.4 we summarize the results found in the current section.

3.1 The Model and Simulation Details

In this section, we will investigate the dynamical properties of a two-dimensional system, composed of N monodisperse active particles, which interact via a dipole-dipole potential. The interaction potential is

$$U(r_{ij}) = U^{SC}(r_{ij}) + U^{D}(r_{ij}), \tag{3.1}$$

where r_{ij} is the distance between particles i and j, U^{SC} denotes a short-range soft core potential and U^{D} a dipole-dipole pairwise interaction potential. The explicit expressions for these potentials are

$$U^{SC}(r_{ij}) = \varepsilon \left(\frac{D}{r_{ij}}\right)^{n} \tag{3.2}$$

and

$$U^D(r_{ij}) = \varepsilon \frac{\mu^2}{r_{ij}^3}[\hat{u}_i \cdot \hat{u}_j - 3(\hat{u}_i \cdot \hat{r}_{ij})(\hat{u}_j \cdot \hat{r}_{ij})], \tag{3.3}$$

where μ is the modulus of the magnetic moment of the particle, $\hat{u}_i$ is the orientation of the particle i, and n control the hardness of the spheres, D is the diameter of the particle, and a hat over a vector denotes a normalized vector. ε and D are defined to be the unit of energy and length, respectively. The parameters used in this section are summarized in Table 3.1.

A schematic plot of the interpaticle potential is seen in Fig. 3.1, where the roman numbers relate the potential curve to the particle configuration on the right side of the figure. In the latter, we observe that the energy presents a strong dependence on the particles' orientations. Namely, the system can be found in a bounded state only in configurations (III) and (VIII), where the latter is the ground state. For this reason, the particles tends to align into chains of particles.

The potential associated with the magnetic field is

$$V = -\vec{\mu}_i \cdot \vec{H}, \tag{3.4}$$

where $\vec{H}$ is the external magnetic field. During this work, the magnetic field will be aligned with the y-axis.

The dipolar potential and the magnetic field generate torque on the particles. The interparticle potential makes particles align with each other, while the magnetic field tends to align the particles with the y-axis. The torques are given by

$$\tau_{ij}^D = \frac{\mu^2}{r_{ij}^3}\left[3(\hat{u}_i \times \hat{r}_{ij})(\hat{u}_j \times \hat{r}_{ij}) - \hat{u}_i \times \hat{u}_j\right], \tag{3.5}$$

$$\tau_i^H = \vec{\mu}_i \times \vec{H}. \tag{3.6}$$

Applying equations 3.2 and 3.3 on Eq. 2.1, we obtain

$$\vec{F}_{ij}^{SC}(r_{ij}) = 12\frac{D}{r_{ij}^{13}}\vec{r}_{ij}, \tag{3.7}$$

Figure 3.1 Interparticle potential defined by Eq. 3.1 for several particle configurations, as indicated in the right side of the figure. Depending on the orientation of the particles, the system can transition between a bound state and an unbounded one.

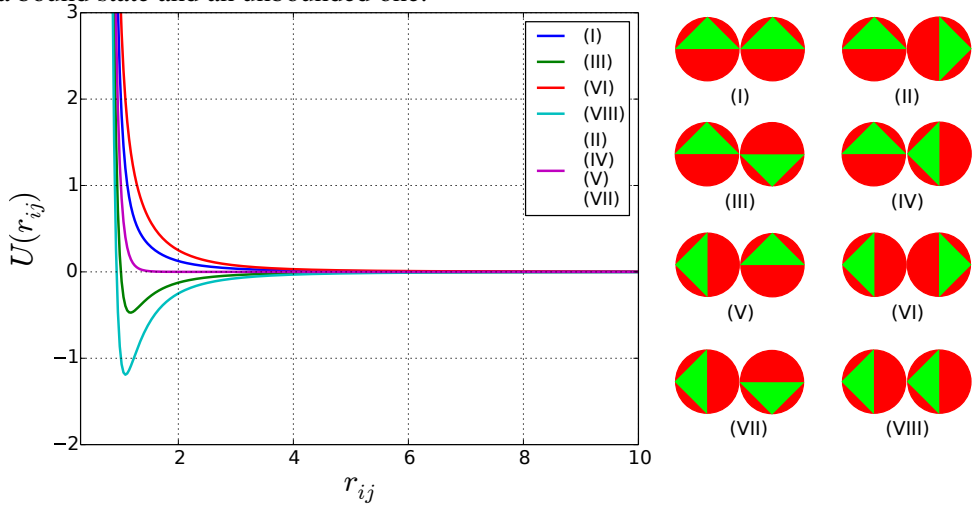

and

$$\vec{F}_{ij}^{D}(r_{ij}) = \frac{3\mu^2}{r_{ij}^4}\left[(\hat{u}_j\cdot\hat{r}_{ij})\hat{u}_i + (\hat{u}_i\cdot\hat{r}_{ij})\hat{u}_j) + (\hat{u}_i\cdot\hat{u}_j)\hat{r}_{ij}\right] - \frac{3\mu^2}{r_{ij}^4}\left[5(\hat{u}_i\cdot\hat{r}_{ij})(\hat{u}_j\cdot\hat{r}_{ij})\hat{r}_{ij}\right], \tag{3.8}$$

with the total force on particle i being given by

$$\vec{F}_i = f\hat{u}_i + \sum_j \left(\vec{F}_{ij}^{SC} + \vec{F}_{ij}^{D}\right), \tag{3.9}$$

where the first term on the right hand side is responsible for the self propulsion of the particle. In the current section, the propulsion and the magnetic moments are aligned within a particle and f is set to unity. A similar situation, where the propulsion and dipolar moments are aligned, is found on the magnetotactic bacteria (BLAKEMORE, 1982; ARAUJO et al., 1990).

We would like to note that, while we adopt the notation of magnetic dipoles (and explicitly refer to the active particles as *magnetic* throughout the text), the energy equations for both, electric and magnetic dipoles are analogous. This means that the results obtained in this work are valid for any dipole-like particle, be it of electric or magnetic nature (JACKSON, 1975).

To model both, the translation and rotational movements, we will use the overdamped Langevin equation, given by Eq. 2.7. That is, our equations of movement will be

$$\frac{dr_i}{dt} = F_i(t) + \eta(t), \tag{3.10}$$

and

$$\frac{d\theta_i}{dt} = \tau_i(t) + \xi(t), \tag{3.11}$$

where we have set $\gamma = 1$. In the same way as Eq. 3.9, the total torque on particle i is given by

$$\tau_i = \tau_i^H + \sum_j \tau_{ij}^D. \tag{3.12}$$

To integrate Eqs. 3.10 and 3.11, we used the algorithm described in Subsection 2.3. Initially the particles were distributed in a squared grid with a random orientation following an uniform distribution in the range $[0, 2\pi)$. The simulation ran for a total of $N_{Steps} = 6 \times 10^6$ time steps where the system was allowed to stabilize for 3×10^6 time steps. This value was chosen after careful examination of the convergence of the measured properties of the system and a wide margin of subsecurity was given. In that way, we avoid any influence of transient effects in our measurements. The simulations were performed in a square box with size $L = 50$ with periodic boundary conditions in both x and y axis.

In order to compare the results in this dissertation with experimental values, one must connect the dimensionless values presented to the real ones. This can be done by setting a few, basic units, and deriving the interesting quantities from the relations necessary to adimensionalize the final Hamiltonian. Using this procedure, one can find that having chosen, for instance, the unit of length, $\bar{r}$, the unit of mass $\bar{m}$, and the unit of dipolar moment, $\bar{\mu}$, it is possible to calculate the unit of time as $\bar{t} = k_{e,m}\bar{r}^2/\bar{\mu}$, the unity of energy $\bar{\varepsilon} = k_{e,m}\bar{\mu}^2/\bar{r}^2$ and the unit of external field $\bar{H} = k_{e,m}\bar{\mu}/\bar{r}^2$. In the previous equations, $k_{e,m}$ stands for the electric and magnetic constants, $k_e = 1/4\pi\varepsilon_0$ and $k_m = \mu_0/4\pi$.

Iron(II) Oxide, for instance, has a molecular weight of 71.844g/mol and a density of 5.745g/cm^3 (PATNAIK, 2003) and each FeO group carries around 5D[1]. Colloidal particles made with this compound, have a diameter anywhere from 10nm to 100nm (HOU; XU; SUN, 2007). Thereby, for particles with diameter around 10nm, we can estimate the mass of each particle as 3.01×10^{-21}kg and a dipole moment up to 4.20×10^{-25}Cm, if we suppose that all the domains are properly aligned. In that way, we can choose our units to be $\bar{m} = 3.01 \times 10^{-21}$kg, $\bar{r} = 10$nm

[1] Here D denotes Debye, the cgs unit for electric dipole. Its SI value is 3.336×10^{-30} Cm.

Table 3.1 Parameters used in this section's simulations, given in dimensionless units.

Parameter	Value
N	384
L	50
D	1
ϕ	0.12
ε	1
n	12
δt	$5 \cdot 10^{-4}$
μ	1.0, 2.0, 3.0
H	[0.0, 0.5]

and $\bar{\mu} = 10^{-25}$Cm, and use the equation in the previous paragraph to calculate any quantity. For instance, the external field unit is found to to be $\bar{H} = 8.99V$.

3.2 Order Parameters

In order to quantify the dynamical properties of the system, we will use a few quantities. The first of these will be the mean squared velocities, defined as

$$\left\langle v_y^2 \right\rangle = \frac{1}{N} \sum_i^N \left(\frac{1}{t} \sum_{t_m}^t v_{iy}(t_m) \right)^2, \tag{3.13}$$

and

$$\left\langle v_\theta^2 \right\rangle = \frac{1}{N} \sum_i^N \left(\frac{1}{t} \sum_{t_m}^t v_{i\theta}(t_m) \right)^2, \tag{3.14}$$

where $v_y(t_m) = \frac{y(t_{m+1}) - y(t_m)}{t_{m+1} - t_m}$, $v_\theta(t_m) = \frac{\theta(t_{m+1}) - \theta(t_m)}{t_{m+1} - t_m}$. Additionally, t_m iterates over the measurements, and we set the time interval between two consubsecutive measurements to be $200\delta t$. That is, $t_m \in \{0\delta t, 200\delta t, 400\delta t, \cdots\}$. In a system composed of auto-propelled particles described by Eq. 3.11 with no interactions, the equations of motion for a single particle are

$$\frac{dx}{dt} = v_x = f \cos\theta \tag{3.15}$$

and

$$\frac{dy}{dt} = v_y = f \sin\theta. \tag{3.16}$$

Thus, in an ensemble of free self-propelled particles, we expect to find $\left\langle v_y^2 \right\rangle = \left\langle f^2 \sin^2\theta \right\rangle = f^2/2$. However, if these particles are now allowed to interact with an external magnetic field as described above, it will be energetically favourable to align with the y-axis. This has the effect of nullify v_x while maximizing v_y, that is, $\left\langle v_y^2 \right\rangle = f^2$. In that way, by using the mean squared velocity we might be able to differentiate between the several configurations that will occur.

Some authors also measure the diffusion of the particle. The quantities in our interest would be the angular diffusion and the diffusion in the y direction. These are given by

$$D_y(t) = \frac{1}{2Nt} \sum_i \left(y_i(t) - y_i(0)\right)^2, \tag{3.17}$$

$$D_\theta(t) = \frac{1}{2Nt} \sum_i \left(\theta_i(t) - \theta_i(0)\right)^2, \tag{3.18}$$

Lets take a moment to analyse the long-time behaviour of $D_y(t)$ for two selected systems. The first system we will analyse will be that composed of Brownian (also called passive) particles. For an ensemble composed of those particles, $\left\langle y^2 \right\rangle \to 2Dt$ (FEYNMAN; LEIGHTON; SANDS, 1963), where D is translated to $\gamma k_B T$ in Eq. 2.6. Therefore,

$$D_y(t) = \frac{1}{2t} 2Dt = D, \tag{3.19}$$

is a constant. However, our system contains active, rather than passive particles. At low temperature a free active particle will drift with a constant speed. Its movement equation will be

$$\frac{dy}{dt} = f \sin(\theta) = f', \tag{3.20}$$

which has the trivial solution $y(t) = f't + y(0)$. Therefore, for an ensemble of free active particles,

Figure 3.2 Schematic representation of particles. In (a) they face the same direction thus being considered neighbors, while in (b) they do not face the same direction and are not neighbors.

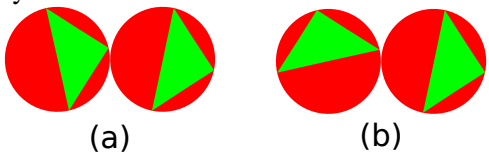

$$\begin{aligned} D_y(t) &= \frac{1}{2t}\left\langle (f\cos(\theta)t)^2 \right\rangle \\ &= \frac{1}{2t} f^2 t \left\langle \cos^2(\theta) \right\rangle, \\ &= \frac{f^2 t}{4}. \end{aligned} \tag{3.21}$$

Thus, due to the self propulsion, we expect to find a D_y constant only when the system is somehow bound. For an interacting system $D_y(t) \sim \beta t^{\alpha}$, where α will have value in the interval [0,1].

However, this quantity is more complex than the mean squared velocity, and while we did measure it for this section's simulations, they provided no new information.

We observed in some simulations the occurrence of small, short lived clusters, as seen in Fig. 3.4 (a) and Fig. 3.6 (a).

In order to identify these clusters, we devised the following algorithm. First, we calculated the interparticle distances r_{ij}, and initially considered any pair of colloids with $r_{ij} < 1.5D$ as neighbors. Due to the angular nature of the interaction potential in this work, we could not use only the proximity factor to must define an angular condition to complement our neighborhood condition. That is, we filtered the neighbor list, selecting those particles that face the same general direction as being neighbors. We tested various values of angular distance as the filtering condition and found a robust value to be $\pi/2$. In that way, the two particles in Fig. 3.2 (a) are considered neighbors, while the particles in (b) are not.

This allowed the creation of a graph of neighbors, with the particles as vertexes. Where we identify each disjoint subgraph as a cluster. We measured the average size of the clusters as the average number of particles in each cluster.

Measuring the lifetime of the cluster, however, is far trickier than measuring its size, as it involves solving the ontological problem of what constitutes the entity and whether it did change or go out of existence.

We tracked the clusters in the following manner. Initially, we identify the clusters and

choose them as *model-clusters*. At each measurement step, we check if each model-cluster is similar to the new clusters. If so, the model-cluster is still considered active. Otherwise its lifetime is saved, and it is considered dead. Any new cluster that does not correspond to any similar model is considered a new model-cluster and its creation time is saved. We define that two clusters A and B are similar if half of the particles in A are also in B. This condition was robust, in that, while we arbitrarily chose the continuity condition as 50%, the measurements did not change greatly for reasonable variables on this value.

Finally, in order to account for possible growth of the clusters, we consider a cluster that is similar to and larger than a model-cluster as the new model-cluster, inheriting its predecessor creation time stamp. We then consider the old model-cluster dead, but its lifetime is not measured. In the occasion that two clusters merge, the smaller one is considered dead, and its lifetime is saved.

3.3 Results

In this subsection we will investigate how the values of μ and H influence the dynamics of the system. We simulate system of $N = 384$ particles, with filling factor $\phi = N\pi D^2/4L^2 = 0.12$.

We also ran a few tests with $N = 1152$ and did not observe any new behaviours. Thus, we expect that simulations with $N = 384$ should be representative of the real system and provide a good balance between fidelity and computational effort.

We investigated the magnetic field and the dipole moment in the ranges $0.0 \leq H \leq 0.5$ and $0.0 \leq \mu \leq 3.0$. We observed that the system saturates for $H > 0.5$, with no new structures arising after that value. Unfortunately, we could now simulate systems with $\mu > 3.0$, due to numerical instabilities. To tackle this issue, we would need to use a much smaller time step δt, incompatible with our computational resources.

In the simulated ranges, we could identify a few distinct structures, such as annular formations, unordered motions and labyrinths. These structures mirror the known orderings for two-dimensional dipole-like colloids (HELGESEN et al., 1988; SCHMIDLE et al., 2012).

Figure 3.3 shows the values of $\langle v_\theta^2 \rangle$ and $\langle v_y^2 \rangle$ for a few values of μ and varying values of H, calculated via Eqs. 3.13 and 3.14, respectively. In Figure 3.3 (top) we can observe two effects. Firstly, we notice that for low magnetic fields, systems with $\mu = 1.0$ and $\mu = 2.0$ have nearly no angular velocity. Indeed, $\langle v_\theta^2 \rangle$ in these systems diverges from those of systems with $\mu = 3.0$ by nearly an order of magnitude. Second, one can observe in Figure 3.3 (bottom) that for most values of H, systems with intermediate value of magnetic dipole moment, i.e., those

with $\mu = 2.0$, are more aligned with the y-axis than systems with either extremal $\mu = 1.0$ and $\mu = 3.0$.

Both effects described in the last paragraph stem from the same source: the energetic competition between the interparticle potential, which depends on the square of magnetic dipole moment, and the external potential, which varies linearly with μ and the angular noise.

Figure 3.3 Mean squared velocities (MSV) for some values of μ and varying H, as indicated within the figures. (top) presents the angular MSV, while (bottom) presents the MSV in the y-axis, that is, parallel to the magnetic field.

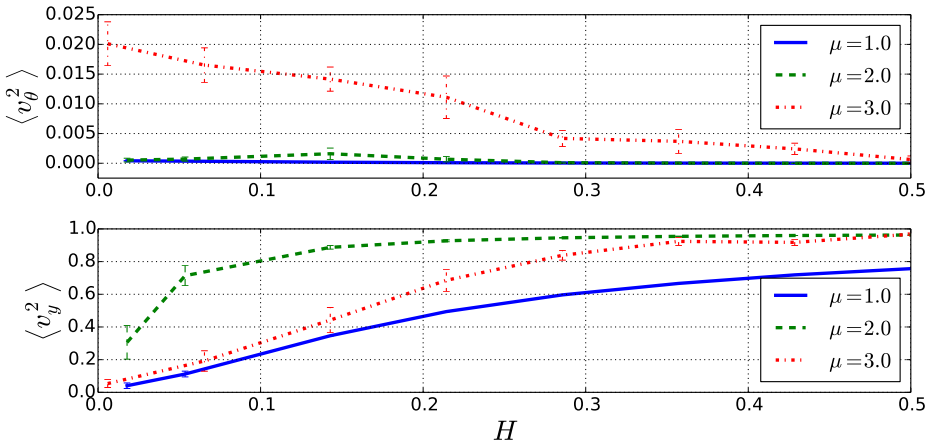

For instance, when $\mu = 1.0$, the angular noise is strong enough to destabilize any potential structures, allowing only short-lived lines to form and preventing the system from aligning properly with the magnetic field, as seen in Fig. 3.5 (a). Indeed, the average lifespan of the string is $(4.2 \pm 0.4) \times 10^3 \delta t$ and contains in average 3.7 ± 0.2 particles.

As we increase the value of μ to 2.0, most of the particles align with the external field. But, if we increase the value of μ further, the dipole-dipole interaction becomes energetically favourable, and the particles will align among themselves, rather than with the external field. This is the reason why systems with dipole moment $= 2.0$ present the highest MSV in the y-axis, as seen in Fig. 3.3 (bottom). The high angular velocity for $\mu = 3.0$ can be explained by the ring structures described in the following subsubsection.

For didactic purposes, in the next two subsubsections we will focus on the extreme conditions of $H = 0$ and $H = 0.5$, as the structures mentioned on the first paragraph of this subsection are more easily seen in these regimes. We did not observe different phenomena for intermediate strengths of the magnetic field. Rather, these systems will gradually align with the external magnetic field and will present structures of both extremes, in proportion to the value of the magnetic field.

3.3.1 Null Magnetic Field: $H = 0.0$

Lets analyse systems with no external magnetic field. In Figure 3.4 we present snapshots of the configurations for a few values of μ. The particles are shown in red, with a green triangle pointing towards the direction of the magnetic moment of each particle. For $\mu = 1.0$, the system has nearly no structure at all (see Fig. 3.4 (a)), presenting only short-lived strings of particles. As we increase μ, these lines stabilize, and their length increases. At $\mu = 2.0$, they coalesce into long lines and often percolate, as shown in Fig. 3.4 (b). As more lines are formed, the line-line interaction tends to align them in a single direction.

Figure 3.4 Formation of dipole rings for a null field. For $\mu = 1.0$ (a), the system has little structure, being in a liquid-like state. When the value of μ is increased to 2.0, we start to see the formation of lines, which percolate. Finally, for $\mu = 3.0$ (c), the system assembles into rings.

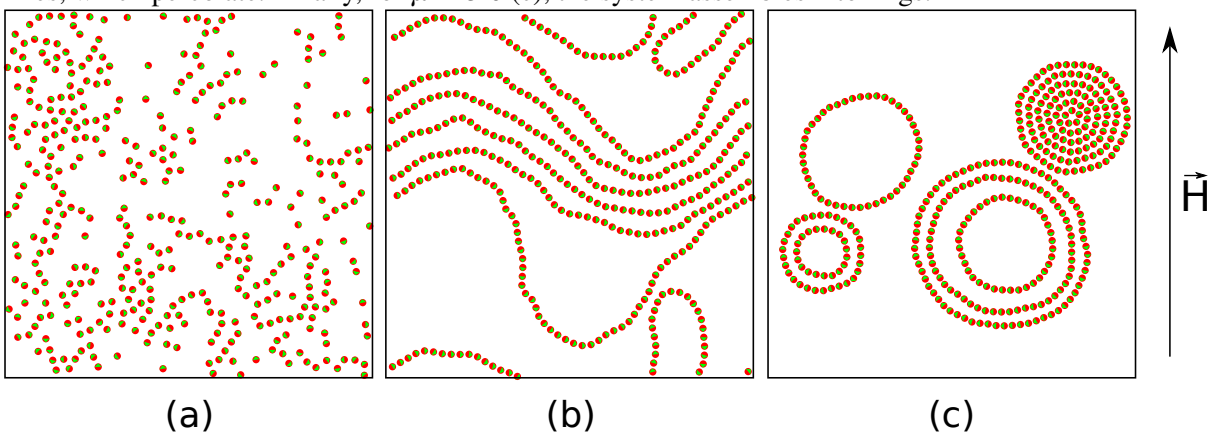

Finally, by increasing μ even further one increases the lines' self-interaction, leading to the destabilization of the strings, which results in the ringed structures seen in Fig. 3.4 (c). These rings are stable rotating structures that, if not disturbed by external forces, keep their shapes indefinitely. As such, they are responsible for the high angular velocity observed in Figure 3.3(a).

3.3.2 Magnetic Field $H = 0.5$

In this subsection, we will discuss the dynamics of systems embedded in a strong magnetic field, with value $H = 0.5$. In this scenario, we observe a movement predominantly on the positive y-direction, as expected due to the energetically favourable alignment between the particles and the magnetic field. Here, the dynamics of particles with $\mu = 1.0$ are similar to those in the previous subsubsection, that is, they also are dominated by short-lived structures.

However, due to the strong magnetic field, they align in a single direction and, by transitivity, among themselves. This alignment allows for a longer, but still finite, life for the strings.

In Fig. 3.5 we present a quiver plot of two systems, both with $\mu = 1.0$, but with different magnetic field magnitude. That is, in (a) we show a system with $H = 0$, while in (b), $H = 0.5$. In this figure, the arrows represent the velocity of the particles, with the speed being represented by the length of the arrow. By contrasting Fig. 3.5 (a) and (b) it is easy to notice that, while both systems are formed by unstable strings of particles, the influence of the magnetic field alone is enough to create longer lines.

We observed a nearly two fold increase in the average life span of strings when compared with systems at null magnetic field, from $(4.2 \pm 0.4) \times 10^3 \delta t$ to $(7.3 \pm 0.9) \times 10^3 \delta t$. The average number of particles per string also increased, to (5.1 ± 0.3).

Figure 3.5 Quiver plot of velocities for two systems with $\mu = 1.0$. In (a), $H = 0.0$, and in (b), $H = 0.5$. In these plots, the length of the arrow is proportional to the speed of the particle.

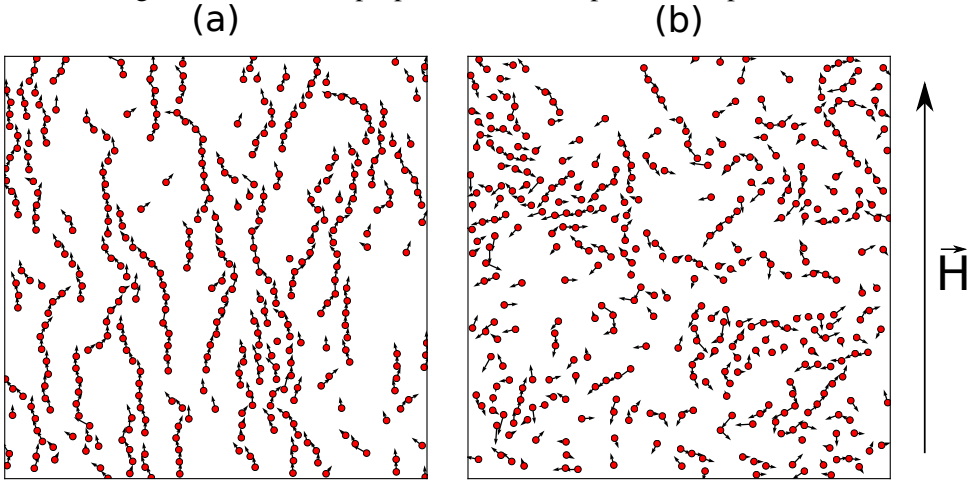

When we increase the value of the magnetic moment, the lines observed in Fig. 3.4 (b) align with the magnetic field, as seen in Fig. 3.6 (b). One thing to be noted, is that some of the lines have bifurcations, forming labyrinths. As we increase the value of the particles' magnetic moment, these bifurcations grow in number, creating highly-branched structures such as the one seen in the right-most part of Fig. 3.6(c). The structures in (c) seems to share its topology with the diffusion-limited aggregation (DLA). It is know that a cluster of interacting colloids would assemble into a DLA cluster in the abscense of a magnetic field (PASTOR-SATORRAS; RUBÍ, 1995). However, reliably measuring the fractal dimension of these clusters was out of the scope of this MSc. Thesis.

Figure 3.6 Formation of labyrinths. For $\mu = 1.0$ (a), the particles assemble into short and fast-lived strings. As μ is increased to 2.0 (b), percolated lines and bifurcations on these lines are found, forming labyrinthine structures. In (c) we can see a system with $\mu = 3.0$. In this system, the line-line interaction compresses them.

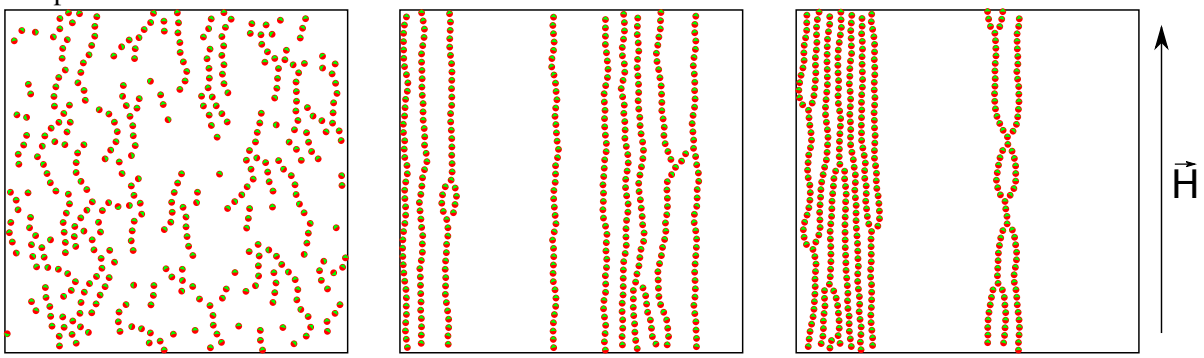

3.4 Summary of Section

In this section, we used Langevin dynamics to investigate the dynamical structures of self-propelled particles in two dimensions, assuming they interacted via a short range hard-core potential and a longer range dipole-dipole potential. We found that the system can organize into various configurations, depending on the dipole magnetic moment and the magnetic field.

In the absence of magnetic fields, the system could be found in a disordered, liquid-like state, comprised of short-lived strings of particles. In systems with stronger magnetic dipole moments, percolated lines and annular structures were also obtained.

The dynamics of the system can be strongly influenced by an external magnetic field, breaking the symmetry of the system. The influence of the magnetic field makes the particle alignment in the y-axis energetically favourable, collimating the percolated lines and destroying the rings obtained at null magnetic field. A Secondary effect of the magnetic field is extending the life expectancy of the strings of the disordered states.

The transition between the null magnetic field regime and the high magnetic field regime was continous. That is to say, at intermiate magnetic fields, we could observe structures belonging to both regimes, and no new phenomena were observed.

4 Transport of passive matter

(. . .) vêm e vão, vão e vêm, até que ficam.

—JOSÉ SARAMAGO (O Homem Duplicado)

In medicine, one of the current challenges is that of vectorization, which consists of the careful delivery of chemical compounds to a specific organ, tissue or even cell. The vectorization process, maximizes the drug potency while decreasing its toxicity, which ensures maximum treatment safety (SOUSSAN et al., 2009). The knowledge of how self-propelled materials behave in the presence of passive matter may assist in developing this application even further.

In Section 3 we encountered several dynamical structures. We found that the resulting phase of system depends on both, intrinsic characteristics of the particles (such as its dipole moment) and extrinsic factors (for instance, the external magnetic field).

Among the structures found, the most promising to transport passive matter was the labyrinthine structures and its associated pockets, mentioned in Subsec. 3.3.2. It is possible that these pockets can envelope the passive particles and transport them in the direction dictated by the external magnetic field.

In this section, we will investigate whether it is possible to take advantage of the structures found in the previous section to transport passive matter.

4.1 Modifications to the model

We introduce N_P passive particles in our simulation. These particles interact via hard-core potential, given by Eq. 3.2, and are not self-propelled. Their equation of movement is

$$\frac{dr_i^P}{dt} = F_i^P(t) + \eta(t) \tag{4.1}$$

where

$$\vec{F}_i^P = \sum_j^{N_A} \vec{F}_{ij}^{SC} + \sum_j^{N_P} \vec{F}_{ij}^{SC}, \tag{4.2}$$

and F_{ij}^{SC} is given by Eq. 3.7, and superscripts A or P indicate if the equation is related to active or passive particles. Similarly, Eq. 3.9 is modified to

$$\vec{F}_i^A = f\hat{u}_i + \sum_j^{N_A} \left(\vec{F}_{ij}^{SC} + \vec{F}_{ij}^{D} \right) + \sum_j^{N_P} \vec{F}_{ij}^{SC}. \tag{4.3}$$

The passive particles are isotropic, thus their orientation is not relevant for the Hamiltonian and do not interfere in the dynamics of the system. For that reason, it is superfluous and was not simulated.

The simulations were realized in a similar manner as those in Section 3. First, the passive particles were assigned to random sites of a square grid. Secondly, the active particles were distributed in the remaining sites and oriented randomly. The system then was allowed to stabilize for 3×10^6 times steps and the measurments were realized in the next 3×10^6 time steps. Except where explicitly noted otherwise, the simulation parameters are the same as in the previous section, which were summarized in Table 3.1.

In passive systems, it is well know that solutions of dipolar colloids at high density can crystallize into a solid (SCHMIDLE et al., 2012). For this reason, we study systems with both, low and high filling factors. These systems present distinct dynamics and transport capabilities, which will be presented in the next two subsubsections.

4.2 Low filling factor

We begin this part of the investigation by adding $N_P = N = 384$ passive particles into the system. Thus, the filling factor doubles, reaching $\phi = 0.24$. Tests were also conducted with $N_P = 128$ and $N_P = 256$, with similar results.

Figure 4.1 shows the mean squared velocity on the y-axis for both kinds of particles, active and passive, denoted by $\langle v_y^2 \rangle^A$ and $\langle v_y^2 \rangle^P$, respectively. The curves for the active particles are very similar to those in Fig. 3.3 (bottom), while for weaker magnetic fields the systems with $\mu = 2.0$ are able to have a better alignment with the y-axis than those systems with $\mu = 1.0$ or $\mu = 3.0$. However, our initial expectations that the labyrinths could sweep the passive particles were not met. Such a factor is demonstrated in Figure 4.1 (bottom), which shows that only systems with $\mu = 1.0$ transport passive matter, and even so, very slowly. In fact, the maximum

Figure 4.1 Mean squared velocity for active (top) and passive particles (bottom). The kind of particle is denoted by a superscript A or P. The active particles' MSV does not differ qualitatively from Fig.3.3 (top). However, the mean squared velocity for passive particles shows that only systems with a small magnetic dipole moment transport passive particles.

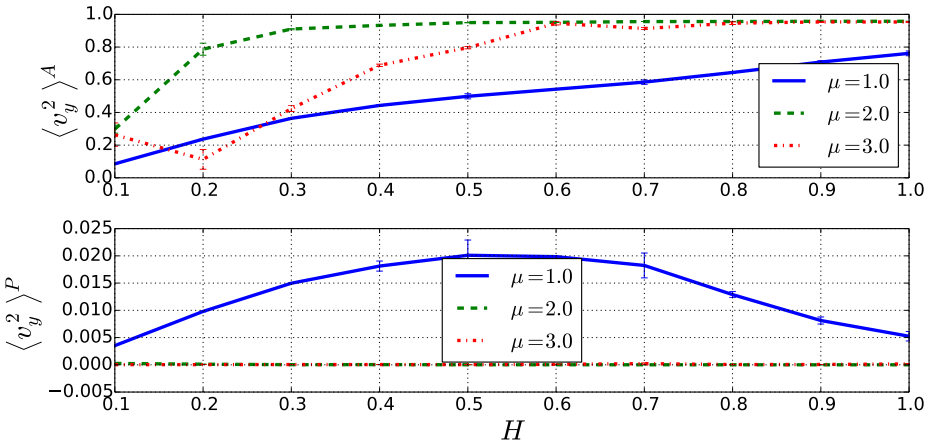

MSV in this case is 0.020.

The pockets in the labyrinths have little use in the transport of passive particles, as the dipole-dipole interaction at the bifurcation isn't strong enough to hold the passive matter. We found that microscopically, the actual process of transport is done by collisions between active and passive particles. As the particles with large magnetic moment assemble into labyrinths, the collision mechanism is minimized.

The difference between the cross section of the liquid-like state and that of the labyrinths is exemplified in Figure 4.2. In this figure we show the active particles in red and the green triangles indicate the direction of the magnetic dipole moment while the passive particles were painted in blue.

We can see a clear mixing of active and passive particles in Fig. 4.2 (a), where the passive particles obstruct the movement of the active particle, resulting in a MSV smaller than in systems with magnetic dipole moment $\mu = 2.0$ or $\mu = 3.0$. In these later two systems, there is a separation between the two kinds of particles, with the active particles organizing into the aforementioned labyrinths and the passive particles organize into stripes, as seen in Fig. 4.2 (b) and (c). The mixing of the particle species shown in Fig. 4.2 (a) is responsible for the non-negligible transport of passive particles, as it maximizes the active-passive interface, and consequentially, the frequency of the collisions.

Furthermore, we observe a decrease in the transport capacity of passive particles even for systems with $\mu = 1.0$ when subjected to magnetic fields higher than $H \approx 0.5$. This decreasing

Figure 4.2 Snapshots of systems with (a) $\mu = 1.0$, (b) $\mu = 2.0$ and (c) $\mu = 3.0$ and external magnetic field $\vec{H} = 1.0$. In (a), the system does not present a well defined structure, maximizing the frequency of collisions between active and passive particles. In (b) and (c), the spatial separation between the two kinds of particles is clear, where the active particles assemble into labyrinths and the passive particles assemble into stripes filling the remaining space.

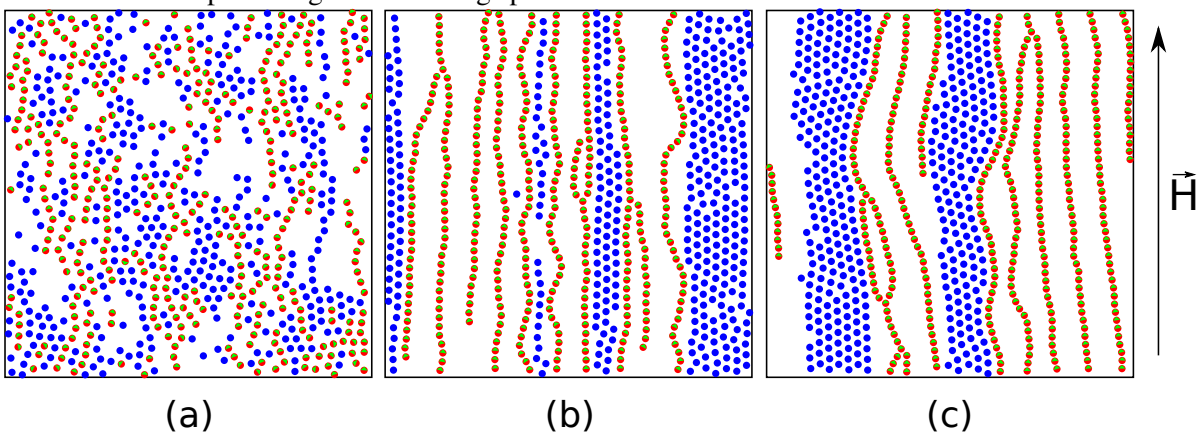

is also due to the alignment of the particles with the external magnetic field, as it reduces the strings cross-section area.

At this point, one may be discouraged to use magnetic particles in passive matter transport, as the mean squared velocity of active and passive matter differ by no less than two orders of magnitude, as seen in Fig. 4.1. We hypothesise that it is possible to overcome this issue by a judicious usage of the reduction in the mean square velocity in systems embedded in magnetic fields stronger than 0.5.

In a finite system one can apply a magnetic field of medium strength (that is, $\vec{H} = 0.5\hat{y}$) until the active particles aggregate on the upper-most part of the cell and then apply a stronger inverted magnetic field (say, $\vec{H} = -1.0\hat{y}$). Once the active matter is now concentrated at the bottom of the cell, the magnetic field is returned to its original state, pointing towards the positive y-axis. By repeating this cycle, one can take the most advantage of the peak in Fig. 4.1 (bottom).

To test this hypothesis, we simulated a cell with PBC in the x-axis and hard walls in the y-axis, with dimensions $L_x = 50$ and $L_y = 100$. All the other parameters are the same as the ones in Table 3.1. All particles start in the lower half of the box, rendering the upper part of box empty. Then, the external magnetic field is set to $\vec{H} = 0.5\hat{y}$.

The system is iterated until more than 50% of the active particles are found in upper 20% of the box. At this point, the magnetic field is flipped, being set to $\vec{H} = -1.0\hat{y}$. The system is once again simulated until the system inverts and most of the active particles concentrate in

Figure 4.3 Percentage of passive particles found in the upper half of the simulation box. In this experiment, the magnetic field is varied between two distinct values, $H = -1.0\hat{y}$ and $H = 0.5\hat{y}$. The moment of alternation is dictated by the number of active particles on each side of the box, as explained in the text.

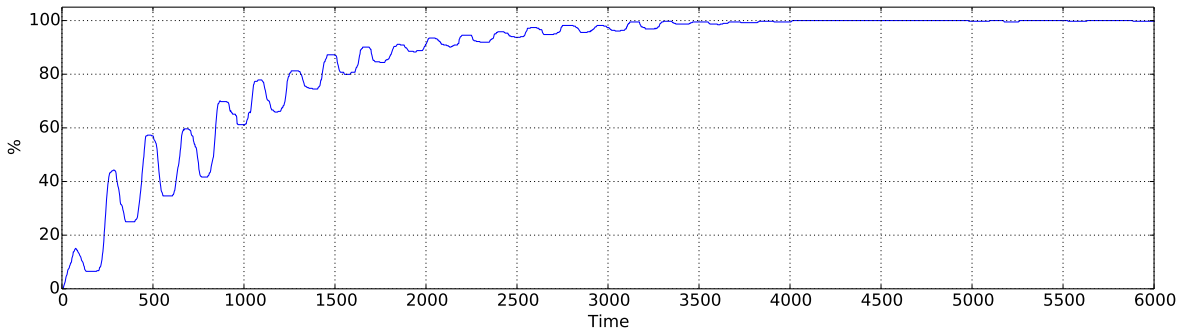

the bottom 10% of the simulation cell. We repeat this procedure until the amount of passive particles in the upper half of the box is fixed.

The result of this computational experiment is shown Fig. 4.3. This figure shows the percentage of *passive* particles in the upper half of the simulation cell. Despite the expected fluctuations, an upwards trend is clearly visible in this figure. This is mirrored in Fig. 4.4, where we see that, despite starting in a mixed state, the passive particles starting mixed with the active particles, they soon are found in the upper box, even if in a disordered state. After a number of cycles, the pressure imparted by the active particles tends to organize the passive matter into a triangular lattice.

In this way, it is possible to physically separate the two kinds of particles into completely different sides of the simulation box, indicating that the alternating-field solution is indeed viable.

4.3 High Filling Fraction

In the previous subsection we observed that in sparse systems the main mechanism of transport of passive particles were the active-passive collisions. However, this tell us little about the transport in denser systems. In these systems, the higher density may force the particles into a crystalline structures, possibly inhibiting the formation observed in the previous section and consequently, allow new mechanisms of transport.

In order to study these new phenomena, we simulated systems with $L = 35$ ($\phi = 0.49$), that

Figure 4.4 System with alternating asymmetrical magnetic field, as indicated in the text. From top to bottom, the snapshots were taken at times $t = 0$, $t = 435$, $t = 525$ and $t = 9145$.

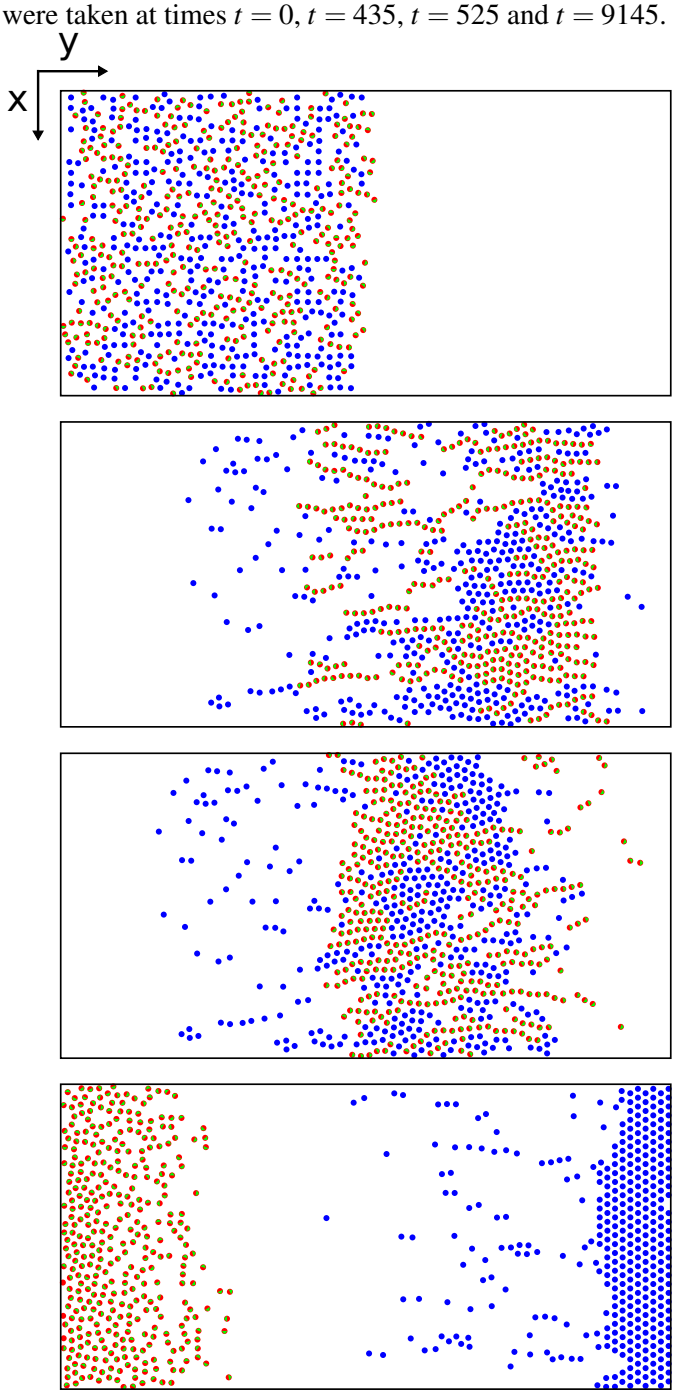

Figure 4.5 Mean squared velocity for active (top) and passive particles (bottom) in a high density environment. On both graphs, we can easily see a separation between MSV systems with $\mu = 3.0$ and those with smaller values of dipole moment. Comparing the values of $\langle v_y^2 \rangle^A$ and $\langle v_y^2 \rangle^P$, one can see that systems with $\mu \leq 2.0$ transport passive particles at a much faster rate than active particles in a dilute system.

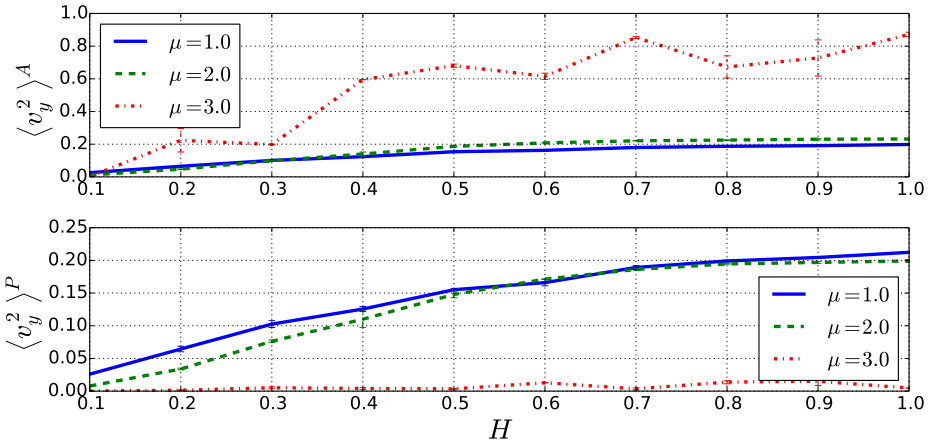

is, dense enough for a system composed solely of passive particles to crystallize.

We show in Fig. 4.5 the mean square velocity of the active and passive particles. The differences between Fig. 4.1 and Fig. 4.5 are striking, with two specially noteworthy effects appearing. First, for systems with magnetic moment $\mu = 1.0$ and $\mu = 2.0$, the value of $\langle v_y^2 \rangle^A$ has decreased to one fifth of their values in Fig. 4.1 (bottom), while $\langle v_y^2 \rangle^P$ has increased by an order of magnitude, bringing the mean squared velocity of the passive particles on pair with those of active particles, at least for the aforementioned values of μ.

This increase can be understood by looking Fig. 4.6 (a), where we observe that the system self-assembles into a triangular lattice, where both kinds of particles are positioned in the lattice sites, moving with the same speed. Despite the presence of some branching between active particle in Fig. 4.6 (b), these lines are imbued in the crystalline structure, rather than in a distinct region. In that way, even systems with $\mu = 2.0$ are in a solid state, and drift nearly in sync.

The second effect is that there is a gap in $\langle v_y^2 \rangle^A$ between the curves with $\mu = 3.0$ and those with $\mu = 2.0$ and $\mu = 1.0$ in Fig. 4.5 (top). This disparity occurs because, unlike systems with smaller dipole moments, for $\mu = 3.0$, the stronger pairwise interaction enables the active particles to overcome the potential barrier. We can see in Fig. 4.6 (c) that particles congregate into different regions, each having a characteristic speed. Moreover, the active particles in Fig. 4.6 (c) organize themselves into a rhombic lattice.

Due to the angular dependence of the dipole-dipole potential, the interaction between two

Figure 4.6 Snapshots of systems with (a) $\mu = 1.0$, (b) $\mu = 2.0$ and (c) $\mu = 3.0$ and external field $\vec{H} = 1.0$. Here we present the quiver plot of the particles' velocities, where both, the length and the colour of the arrows indicate the particles' speed. The colour of the circles are used to distinguish between active (red) and passive (blue) particles. On the top row, we show the whole system and on the bottom row, we show a zoomed version of the region delimited by the dashed box.

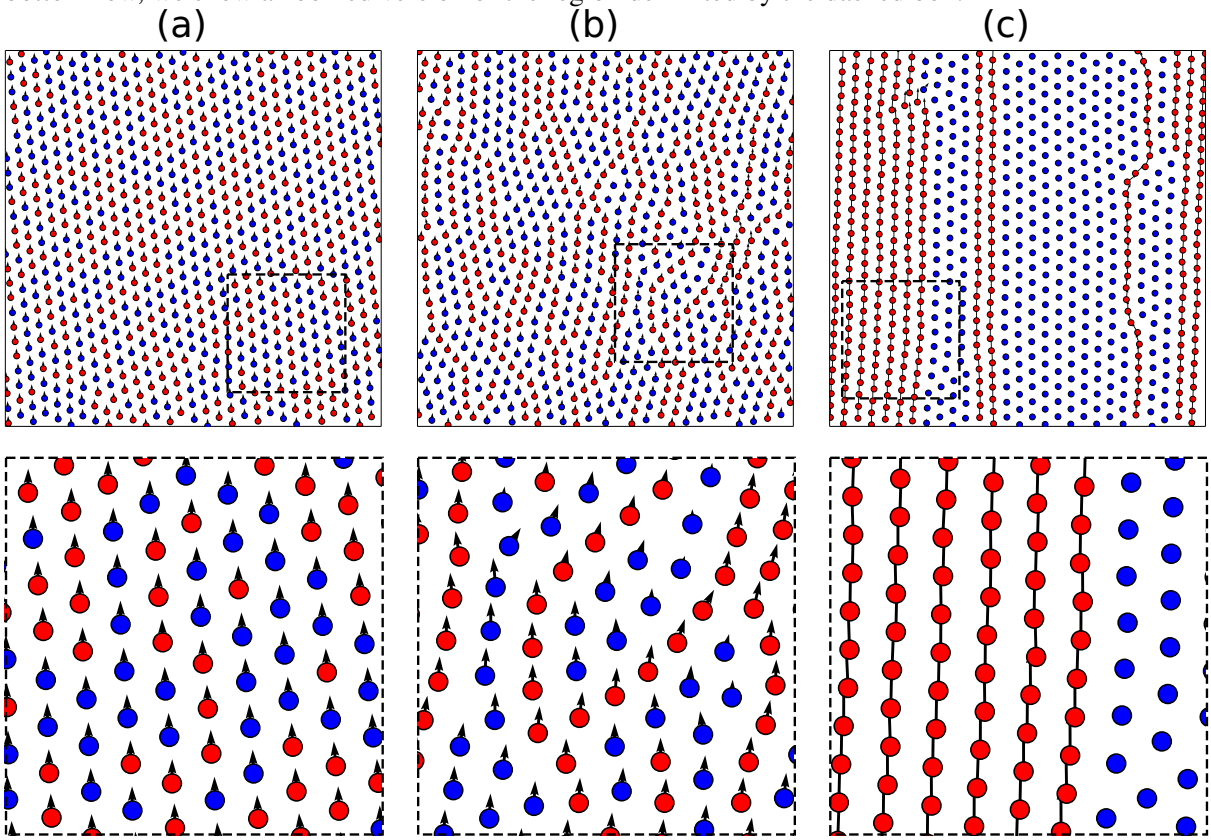

Figure 4.7 Schematic representation of two pairs of lines. In (a), the particles are aligned center-to-center. In (b), there is a step of one radius between particles in each line.

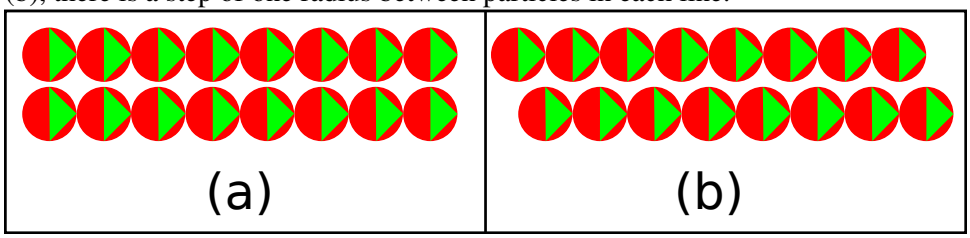

Figure 4.8 Mean squared velocity of active (blue) and passive (green) particles. We observe that the system is in an arrested state until $\mu \approx 1.9$.

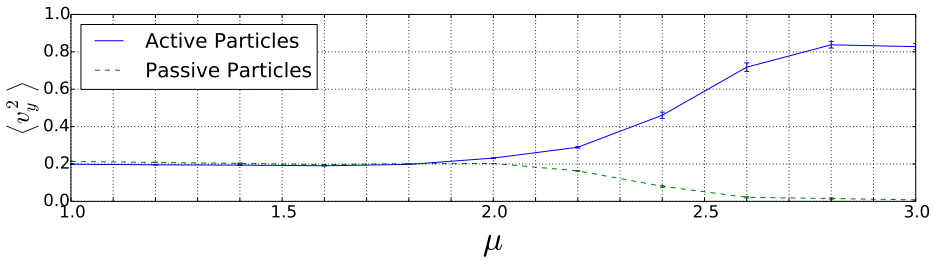

lines can be repulsive or attractive, depending on the pairing of the particles in the two lines. If the particles are perfectly paired, as shown in Fig. 4.7 (a), there will be a net repulsion between the two lines. On the other hand, if there is a misalignment between the particles, the resulting interaction can be attractive. In Fig. 4.7 (b) we see the condition where the attraction reaches the maximum, that is, when the misstep is exactly half of the lines' pitch, thus creating the rhombic lattice observed in Fig. 4.6 (c).

In order to understand the transition from an arrested state to that of localized motion seen in Fig. 4.6, we realized one more set of simulations, but this time keeping $\vec{H}$ constant, with value $\vec{H} = 1.0\hat{y}$, and varying μ in the range $1.0 \leq \mu \leq 3.0$.

In Fig. 4.8 the solid blue line represents the MSV of active particles, and the broken green line represents the MSV of the passive particles. We observe that the system is kept in the frozen state observed in Fig. 4.6 (a) until the dipole moment reaches approximately 1.9. At this point the lines diverge, indicating that active particles start to form veins, such as those observed in Fig. 4.6 (b), which have a larger mobility. As the value of the dipole moment is further increased, the veins' attraction allows them to assemble into the regions observed in Fig. 4.6 (c).

4.4 Conclusions

In this section we investigated systems with a mix of active and passive particles at low and high filling factors. At low filling factors, only active particles with $\mu = 1.0$ were able to transport passive matter. Our initial prediction that the labyrinths would envelope and carry passive particles was not fulfilled. Indeed, we observed that most of the passive particles movement is due to the direct collision between active and passive matter, rather than the envelope-and-sweep mechanism that we had expected.

A disparate dynamics arose in systems in a higher density, where we observed a solidification of the system. In this regime, active particles with $\mu \lesssim 1.9$ were locked into the sites of a triangular lattice, forcing the whole crystal to move synchronously. Particles with a higher magnetic moment were able to overcome the potential barrier created by the passive particles and firstly organizing into veins embedded in the crystal and later into distinct regions.

5 Transport of passive matter by orthogonal active matter

I find the great thing in this world is not so much where we stand, as in what direction we are moving.

—OLIVER WENDELL HOLMES (The Autocrat of the Breakfast Table)

In the previous section, we investigated how active particles could transport passive matter, and discovered that the main transportation mechanism in dilute systems were the direct collisions between the two kinds of particles. Using this mechanism, we showed that, while it is indeed possible to conduct passive matter, this movement was slow and cumbersome, requiring several alternations of the magnetic field.

In the current section, we dwell further in the transport of passive matter in the dilute regime, using active particles whose dipole orientation is orthogonal to its direction of self-propulsion.

In Subsection 1.3, we mentioned several ways to synthesize magnetic particles, including the process of covering a magnetic core with a non-metallic material. We hypothesize that it is possible for a skilled experimentalist to coat the aforementioned particles with a metallic layer, creating Janus Particles (JP). These JPs can then be used as self-propelled particles (GOLESTANIAN; LIVERPOOL; AJDARI, 2005; GOLESTANIAN; LIVERPOOL; AJDARI, 2007). The main advantage of this process would be the fact that the moment of dipole generated by the metallic core and the self-propulsion due to the metallic layering can be chosen in any orientation if the first phase of the synthesis is done carefully.

To simulate these new particles, a complementary change in the model is needed. Now, Eq. 4.3 (which is based in Eq. 3.9) reads

$$\vec{F}_i^A = f\hat{u}_i^{\perp} + \sum_j^{N_A}\left(\vec{F}_{ij}^{SC} + \vec{F}_{ij}^{D}\right) + \sum_j^{N_P}\vec{F}_{ij}^{SC}, \tag{5.1}$$

where $\hat{u}_i^{\perp} = (\hat{u}_{iy}, -\hat{u}_{ix})$. That is, the self-propulsion is orthogonal to the magnetic dipole moment. In previous sections, we calculated the mean squared velocity in the y direction, as it

Figure 5.1 Mean squared velocity for active (top) and passive particles (bottom). The kind of particle is denoted by a superscript A, for active particles, or P, for passive ones.

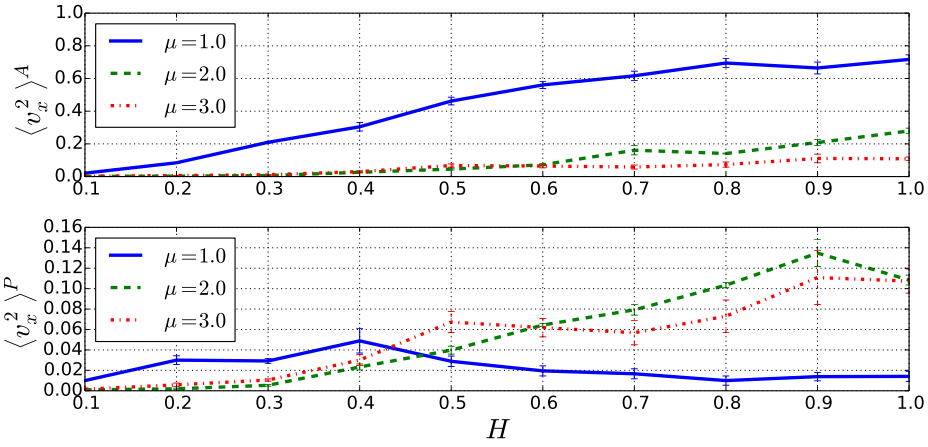

matched the direction of motion of most particles, due to the magnetic alignment between the particles and the magnetic field. Now, as the direction of self-propulsion is orthogonal to the particles' dipole direction, we expect that the movement will happen mostly in the x direction. Therefore, we will calculate $\langle v_x^2 \rangle^D$ and $\langle v_x^2 \rangle^P$ and analyse how it changes as a function of the magnetic field.

For systems with magnetic dipole $\mu = 1.0$, the MSV of the active particles is much larger than that of the passive particles, as seen in Fig. 5.1. Despite the values of $\langle v_x^2 \rangle$ obtained in Fig. 5.1 for systems with $\mu = 1.0$ being similar to those of Fig. 4.1, the transport is not done via collisions, as was the case in the previous section, but rather the active particles sweep the passive ones.

In the column (a) of Figure 5.2 we see that the active particles in systems with $\mu = 1.0$ become organized in strings, that, while perennial (in stark opposition to those found in Sections 3 and 4), are not resilient enough to envelope passive matter.

Increasing the magnetic dipole moment we also strengthen the string, allowing them to transport more passive cargo. In Fig. 5.2 (b), we observe, that, despite the passive particles indeed being transported, the strings are still subject to breakage, which we indicated by the large arrows within the figure.

We learned in Subsec. 3.3.2 that percolated lines can form in systems with $\mu > 2.0$. When the self-propulsion and the magnetic moment are orthogonal, these lines sweep the passive particles, allowing for a greater transport of those particles.

This is also the case seen in systems with high magnetic dipole (that is, $\mu = 3.0$), observed in Fig. 5.2 (c). In this last situation, not only the active particles sweep the passive particles, as

they did in systems with $\mu = 2.0$, but they are also able to envelope them, creating true pockets of passive particles, as indicated by the arrows in Fig. 5.2 (c). Thereby, the most efficient way to transport passive matter when the self-propelled particles' dipole and propulsion are orthogonal is by using particles with high dipole moment. This is the opposite of the results obtained in the previous sections, on which a *smaller* dipole moment resulted in a larger mobility for the passive matter.

Figure 5.2 Snapshots of systems with (a) $\mu = 1.0$, (b) $\mu = 2.0$ and (c) $\mu = 3.0$ with $\vec{H} = 1.0\hat{x}$. In the upper row we present the quiver plot of the particles' velocities, where both, the length and the colour of the arrows indicate the particles' speed. The colour of the circles are used to distinguish between active (red) and passive (blue) particles. In the lower row the active and passive particles follow the same colour code as in the upper row. Furthermore, the active particles are drawn with a green triangle indicating the orientation of the particle's dipole moments.
In (a) we see that the passive particles are clusterized and only a small portion of the active particles are responsible for the clusters movement. On the other hand, in (b) most of active matter carry the passive cluster and in (c) not only they transport passive matter, but also encase the passive particles.

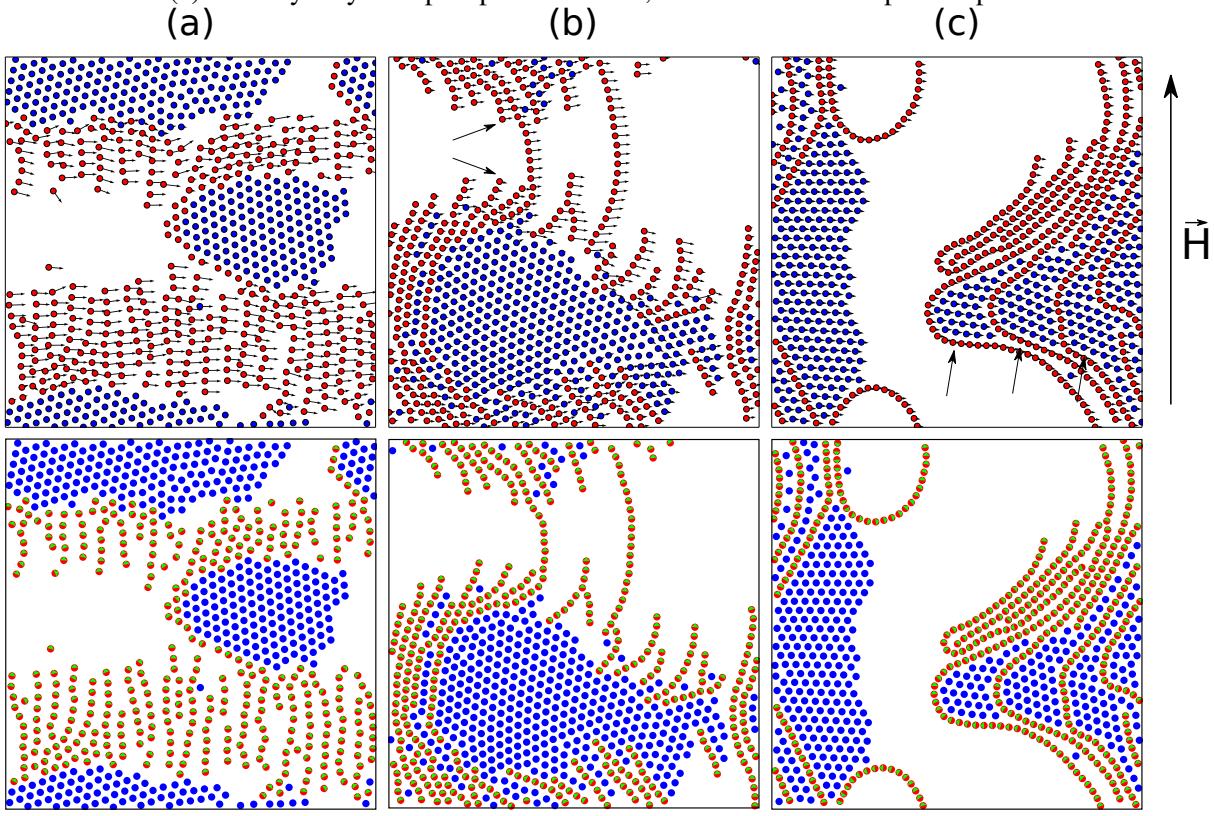

5.1 Conclusion

In this section we investigated the transport of passive particles by active matter whose magnetic dipole moment was orthogonal to the propulsion direction. We observed the rising of a new mechanism of transport, where the lines in Subsection 3.3.2 now sweep and envelope the passive particles. This has the consequence that particles with a higher dipole moment can transport passive matter more efficiently than those with a smaller dipole moment. This is the opposite situation found in the previous section, on which particles with the smallest dipole moment had the best capacity in transporting passive matter.

Indeed, among the studied systems, the particles in this section have the most capacity in the transportation of materials, but at the cost of a possibly more intricate fabrication.

6 Conclusion and Perspectives

"Begin at the beginning," the King said, very gravely, "and go on till you come to the end: then stop."

—LEWIS CARROL (Alice in Wonderland)

In the Introduction of this work, we mentioned that colloids and active matter have several uses, ranging from the pharmaceutical industry to the recovery of waste heat in thermoelectric generators. Inspired by the possibility of vectorization, that is, finely controlled drug delivery, we decided to investigate systems composed of active magnetic particles and their capacity in transporting passive matter. We used Brownian Dynamics to model the solvent-colloid interactions and integrated the resulting equations of motion using a Stochastic Runge-Kutta algorithm.

As the stepping stone for this study, we investigated the structures formed by the magnetic self-propelled particles for various values of external field and dipole moment. In this first part of the work, we expected the particles to be crafted in such a way that the dipole moment and the self-propulsion direction were parallel and we observed several distinct structures arise. In low dipole moments regimes, we encountered intermittent short strings whose lengths could be controlled by a careful choice of the external magnetic strength. When we increased the dipole moment, annular formations began to form in the absence of magnetic fields and branched structures, named labyrinths, formed in the presence of magnetic field.

We observed that the labyrinths had potential use in the transport of passive matter. To test this idea, we prepared systems composed of equal parts of passive and active matter, and studied its behaviour for various sets of parameters both at low and high density. As a result, in systems at low density, we observed was that, contrary to our expectations, the labyrinths were not able to carry passive particles. However, systems with a lower value of dipole moment could transport passive matter, even if at slow rate. This happened because the main mechanism of transport in this situation were the heads-on collisions between the active and passive particles. As shorter strings present a larger total cross section than labyrinths, they increase

the passive particles' mobility. We also observed that the transport capabilities of the strings reach a maximum for magnetic field strength around $H = 0.5$, decreasing after such value. We showed that this decrease can be used to transport passive particles in the presence of an asymmetrically alternating magnetic field.

In dense systems the formation of strings and labyrinths were inhibited, and we observed that, for systems with small dipole moment, the particles crystallized in a triangular lattice, as expected, moving in synchrony. As we increased the value of the dipole moment, the active particles firstly formed veins imbued in the larger crystalline structure and as we further increased the value of the dipole moment, we observed the creation of distinct regions, containing solely active or passive particles, with distinct velocities.

Finally, we studied magnetic particles whose self-propulsion and dipole moment were orthogonal. We found that even at low dipoles moments the transport improved three fold when compared to the previous simulations. Moreover, at high dipole moments, the active particles would truly envelope and sweep passive particles, allowing for a transportation seven times faster than the best case found in systems whose dipole moment was parallel to its self propulsion. Thereby, this has been proven to be the most efficient method to transport passive matter in sparse systems.

Despite the extensive studies we presented in the previous three sections, there are still some important issues to address in systems composed of magnetic active particles. For instance, one topic that can be better understood by further study is the possibility of transportation of passive matter by the labyrinths obtained in Section 3. In a broader inspection of the parameter space, it might be possible to find a set of parameters that would allow the use the pockets in the transportation of passive matter. For instance, decreasing the mass of the passive particles might allow its transportation. A second possibility is to increase the value of μ, increases the mechanic strength of the labyrinths, enabling the sweeping of heavier passive matter. Finally, through a careful assembly process, it is possible to add patchy sites to the magnetic dipoles, thereby increasing not only the particle-particle adherence but also controlling the frequency of branching in the labyrinths.

A complete understanding of the studied system cannot be developed only by an extension of the investigated parameters. Rather, one must also increase the realism of the simulations itself, including, for instance, hydrodynamics interactions between the particles. This can be done firstly by using the Oseen Tensor to construct a force field dependent on the particles' positions and momenta, emulating the interaction between the particles caused by ripples and vortexes in the solvent. Still, in order to simulate all the hydrodynamics effects, one needs to use specialized algorithms that allow the simulation of the two entities, colloids and sol-

vent, by two different methods. For instance, it is possible to simulate the particles using the standard Molecular Dynamics techniques and to simulate the fluid using Lattice-Boltzmann or Multiparticle Collision Methods.

Another natural extension of this study would be the investigation of similar systems in 2.5 and 3 dimensions. The first case comprises systems that, while three-dimension in nature, have their motion in one of the dimensions handicapped. This handicap can be caused, for instance, by external potentials or simply by a simulation box much smaller in one direction than in the other two. An example of a real world 2.5 dimensional system is that of particles in a liquid-air interface, where the gravity pulls the colloids downwards while the buoyancy keeps them on the surface. In that way, the particles have some ability go over or under other particles using the z direction, but not full freedom to move in that direction. In this case, we do not expect major changes in the structures and mobilities, expect, perhaps, in the high density case presented in Section 4.

On the other hand, we expect that realizing full-fledged three dimensional simulation will result in different structures, even if they follow the trend of string-like clusters. Furthermore, we expect that the ability to transport passive particles would be grandly diminished when compared to its two dimensional version, as the passive matter would be able to circumvent the one-dimensional formations favoured by the dipole potential. Thus, new mechanisms of transport might be investigated for three dimensional systems.

References

AB, N. M. *The Nobel Prize in Physics 1926*. 2014. Disponível em: <http://www.nobelprize.org/nobel_prizes/physics/laureates/1926/>.

ALDER, B. J.; WAINWRIGHT, T. E. Phase transition for a hard sphere system. *The Journal of Chemical Physics*, v. 27, n. 5, p. 1208–1209, 1957. Disponível em: <http://scitation.aip.org/content/aip/journal/jcp/27/5/10.1063/1.1743957>.

ALLEN, M. P.; TILDESLEY, D. J. *Computer Simulation of Liquids*. New York, NY, USA: Clarendon Press, 1989. ISBN 0-19-855645-4.

ALVAREZ, C. E.; KLAPP, S. H. L. Translational and rotational dynamics in suspensions of magnetic nanorods. *Soft Matter*, The Royal Society of Chemistry, v. 9, p. 8761–8770, 2013. Disponível em: <http://dx.doi.org/10.1039/C3SM51549D>.

ANDERSEN, H. C. Molecular dynamics simulations at constant pressure and/or temperature. *The Journal of Chemical Physics*, v. 72, n. 4, p. 2384–2393, 1980. Disponível em: <http://scitation.aip.org/content/aip/journal/jcp/72/4/10.1063/1.439486>.

ANGELINI, I. et al. Chemical analyses of bronze age glasses from frattesina di rovigo, northern italy. *Journal of Archaeological Science*, v. 31, n. 8, p. 1175 – 1184, 2004. ISSN 0305-4403. Disponível em: <http://www.sciencedirect.com/science/article/pii/S0305440304000275>.

ARAUJO, F. F. T. de et al. Magnetic polarity fractions in magnetotactic bacterial populations near the geomagnetic equator. *Biophys J*, v. 58, n. 2, p. 549–555, Aug 1990. ISSN 0006-3495. 19431763[pmid]. Disponível em: <http://www.ncbi.nlm.nih.gov/pmc/articles/PMC1280993/>.

ARTIOLI, G.; ANGELINI, I.; POLLA, A. Crystals and phase transitions in protohistoric glass materials. *Phase Transitions*, v. 81, n. 2-3, p. 233–252, 2008. Disponível em: <http://dx.doi.org/10.1080/01411590701514409>.

ASHCROFT, N.; MERMIN, N. *Solid State Physics*. [S.l.]: Cengage Learning, 2011. ISBN 9788131500521.

BASKARAN, A.; MARCHETTI, M. C. Statistical mechanics and hydrodynamics of bacterial suspensions. *Proceedings of the National Academy of Sciences*, v. 106, n. 37, p. 15567–15572, 2009. Disponível em: <http://www.pnas.org/content/106/37/15567.abstract>.

BLAKEMORE, R. P. Magnetotactic bacteria. *Annual Review of Microbiology*, v. 36, n. 1, p. 217–238, 1982. PMID: 6128956. Disponível em: <http://dx.doi.org/10.1146/annurev.mi.36.100182.001245>.

BÖDEKER, H. U. et al. Quantitative analysis of random ameboid motion. *EPL (Europhysics Letters)*, v. 90, n. 2, p. 28005, 2010. Disponível em: <http://stacks.iop.org/0295-5075/90/i=2/a=28005>.

BROWN, R. *A Brief Account of Microscopical Observations Made on the Particles Contained in the Pollen of Plants, and on the General Existence of Active Molecules in Organic and Inorganic Bodies*. [S.l.: s.n.], 1828.

CABUIL, V. Phase behavior of magnetic nanoparticles dispersions in bulk and confined geometries. *Current Opinion in Colloid Interface Science*, v. 5, n. 1â2, p. 44 – 48, 2000. ISSN 1359-0294. Disponível em: <http://www.sciencedirect.com/science/article/pii/S1359029400000364>.

CHATÉ, H.; GINELLI, F.; MONTAGNE, R. Simple model for active nematics: Quasi-long-range order and giant fluctuations. *Phys. Rev. Lett.*, American Physical Society, v. 96, p. 180602, May 2006. Disponível em: <http://link.aps.org/doi/10.1103/PhysRevLett.96.180602>.

CHOWDHURY, A.; ACKERSON, B. J.; CLARK, N. A. Laser-induced freezing. *Phys. Rev. Lett.*, American Physical Society, v. 55, p. 833–836, Aug 1985. Disponível em: <http://link.aps.org/doi/10.1103/PhysRevLett.55.833>.

COUZIN, I. D. et al. Effective leadership and decision-making in animal groups on the move. *Nature*, v. 433, n. 7025, p. 513–516, Feb 2005. ISSN 0028-0836. Disponível em: <http://dx.doi.org/10.1038/nature03236>.

CZIRÓK, A.; STANLEY, H. E.; VICSEK, T. Spontaneously ordered motion of self-propelled particles. *Journal of Physics A: Mathematical and General*, v. 30, n. 5, p. 1375, 1997. Disponível em: <http://stacks.iop.org/0305-4470/30/i=5/a=009>.

DHONT, J. *An Introduction to Dynamics of Colloids*. [S.l.]: Elsevier Science, 1996. (Studies in Interface Science). ISBN 9780080535074.

DRESCHER, K. et al. Fluid dynamics and noise in bacterial cellâcell and cellâsurface scattering. *Proceedings of the National Academy of Sciences*, v. 108, n. 27, p. 10940–10945, 2011. Disponível em: <http://www.pnas.org/content/108/27/10940.abstract>.

EBELING, W.; SCHWEITZER, F.; TILCH, B. Active brownian particles with energy depots modeling animal mobility. *Biosystems*, v. 49, n. 1, p. 17 – 29, 1999. ISSN 0303-2647. Disponível em: <http://www.sciencedirect.com/science/article/pii/S0303264798000276>.

EINSTEIN, A. *Investigations on the Theory of the Brownian Movement*. [S.l.]: Dover Publications, 1956. (Dover Books on Physics Series). ISBN 9780486603049.

ELGETI, J.; WINKLER, R. G.; GOMPPER, G. Physics of microswimmers–single particle motion and collective behavior: a review. *Reports on Progress in Physics*, v. 78, n. 5, p. 056601, 2015. Disponível em: <http://stacks.iop.org/0034-4885/78/i=5/a=056601>.

FEYNMAN, R.; LEIGHTON, R.; SANDS, M. *The Feynman Lectures on Physics*. [S.l.]: Addison-Wesley, 1963. (The Feynman Lectures on Physics, v. 1). ISBN 9780201021165.

FRIEDRICH, B. M.; JÜLICHER, F. Chemotaxis of sperm cells. *Proceedings of the National Academy of Sciences*, v. 104, n. 33, p. 13256–13261, 2007. Disponível em: <http://www.pnas.org/content/104/33/13256.abstract>.

GANDEVIA, B. Historical review of the use of parasympatholytic agents in the treatment of respiratory disorders. *Postgraduate medical journal*, v. 51, n. 7 SUPPL, p. 13–20, 1974.

GANGWAL, S. et al. Programmed assembly of metallodielectric patchy particles in external ac electric fields. *Soft Matter*, The Royal Society of Chemistry, v. 6, p. 1413–1418, 2010. Disponível em: <http://dx.doi.org/10.1039/B925713F>.

GOLDBERG, D. What every computer scientist should know about floating-point arithmetic. *ACM Comput. Surv.*, ACM, New York, NY, USA, v. 23, n. 1, p. 5–48, mar. 1991. ISSN 0360-0300. Disponível em: <http://doi.acm.org/10.1145/103162.103163>.

GOLESTANIAN, R.; LIVERPOOL, T. B.; AJDARI, A. Propulsion of a molecular machine by asymmetric distribution of reaction products. *Phys. Rev. Lett.*, American Physical Society, v. 94, p. 220801, Jun 2005. Disponível em: <http://link.aps.org/doi/10.1103/PhysRevLett.94.220801>.

GOLESTANIAN, R.; LIVERPOOL, T. B.; AJDARI, A. Designing phoretic micro- and nano-swimmers. *New Journal of Physics*, v. 9, n. 5, p. 126, 2007. Disponível em: <http://stacks.iop.org/1367-2630/9/i=5/a=126>.

GRAHAM, T. Researches on the arseniates, phosphates, and modifications of phosphoric acid. *Philosophical Transactions of the Royal Society of London*, v. 123, p. 253–284, 1833. Disponível em: <http://rstl.royalsocietypublishing.org/content/123/253.short>.

GROSSMAN, J. The evolution of inhaler technology. *Journal of Asthma*, v. 31, n. 1, p. 55–64, 1994. PMID: 8175626. Disponível em: <http://dx.doi.org/10.3109/02770909409056770>.

GUTTAL, V.; COUZIN, I. D. Social interactions, information use, and the evolution of collective migration. *Proceedings of the National Academy of Sciences*, v. 107, n. 37, p. 16172–16177, 2010. Disponível em: <http://www.pnas.org/content/107/37/16172.abstract>.

HAILE, J. M. *Molecular Dynamics Simulation: Elementary Methods*. 1st. ed. New York, NY, USA: John Wiley & Sons, Inc., 1992. ISBN 0471819662.

HAMLEY, I. W. *Introduction to soft matter - revised edition : synthetic and biological self-assembling materials*. Rev. ed. [S.l.: s.n.], 2008. ISBN 9780470516096,0470516097,0470516100,9780470516102.

HELGESEN, G. et al. Aggregation of magnetic microspheres: Experiments and simulations. *Phys. Rev. Lett.*, American Physical Society, v. 61, p. 1736–1739, Oct 1988. Disponível em: <http://link.aps.org/doi/10.1103/PhysRevLett.61.1736>.

HIEMENZ, R. R. P. C. *Principles of colloid and surface chemistry*. 3rd ed., rev. and expanded. ed. [S.l.]: Marcel Dekker, 1997. (Undergraduate Chemistry Series). ISBN 0824793978,9780824793975,9780585238647.

HONEYCUTT, R. L. Stochastic runge-kutta algorithms. i. white noise. *Phys. Rev. A*, American Physical Society, v. 45, p. 600–603, Jan 1992. Disponível em: <http://link.aps.org/doi/10.1103/PhysRevA.45.600>.

HOU, Y.; XU, Z.; SUN, S. Controlled synthesis and chemical conversions of feo nanoparticles. *Angewandte Chemie International Edition*, WILEY-VCH Verlag, v. 46, n. 33, p. 6329–6332, 2007. ISSN 1521-3773. Disponível em: <http://dx.doi.org/10.1002/anie.200701694>.

HOWSE, J. R. et al. Self-motile colloidal particles: From directed propulsion to random walk. *Phys. Rev. Lett.*, American Physical Society, v. 99, p. 048102, Jul 2007. Disponível em: <http://link.aps.org/doi/10.1103/PhysRevLett.99.048102>.

INGEN-HOUSZ, J.; MOLITOR, N. C. *Vermischte Schriften physisch-medicinischen Inhalts*. Wien: Wappler, 1784.

ISLAM, N. Colloids in aerosol drug delivery systems. In: FANUN, M. (Ed.). *Colloids in Drug Delivery*. [S.l.]: CRC Press, 2016. cap. 21, p. 479–500.

JACKSON, J. *Classical electrodynamics*. [S.l.]: Wiley, 1975. ISBN 9780471431329.

JOHNSON, L. R. Coming to grips with univac. *IEEE Annals of the History of Computing*, IEEE Computer Society, Los Alamitos, CA, USA, v. 28, n. 2, p. 32–42, 2006. ISSN 1058-6180.

JONES, J. E. On the determination of molecular fields. ii. from the equation of state of a gas. *Proceedings of the Royal Society of London A: Mathematical, Physical and Engineering Sciences*, The Royal Society, v. 106, n. 738, p. 463–477, 1924. ISSN 0950-1207. Disponível em: <http://rspa.royalsocietypublishing.org/content/106/738/463>.

JONES, R. G. et al. (Ed.). *Compendium of Polymer Terminology and Nomenclature*: Iupac recommendations 2008. The Royal Society of Chemistry, 2009. P001-443 p. ISBN 978-0-85404-491-7. Disponível em: <http://dx.doi.org/10.1039/9781847559425>.

LANGEVIN, P. Sur la théorie du movement brownien. *Comptes Rendus de l'Académie des Sciences*, v. 146, p. 530–533, 1906.

LÖWEN, H. Twenty years of confined colloids: from confinement-induced freezing to giant breathing. *Journal of Physics: Condensed Matter*, v. 21, n. 47, p. 474203, 2009. Disponível em: <http://stacks.iop.org/0953-8984/21/i=47/a=474203>.

LÖWEN, H. et al. Colloidal layers in magnetic fields and under shear flow. *Journal of Physics: Condensed Matter*, v. 17, n. 45, p. S3379, 2005. Disponível em: <http://stacks.iop.org/0953-8984/17/i=45/a=025>.

LYNCH, G. C.; PETTITT, B. M. Grand canonical ensemble molecular dynamics simulations: Reformulation of extended system dynamics approaches. *The Journal of Chemical Physics*, v. 107, n. 20, p. 8594–8610, 1997. Disponível em: <http://scitation.aip.org/content/aip/journal/jcp/107/20/10.1063/1.475012>.

MAITLAND, G. et al. Intermolecular forces: Their origin and determination. *Physics Today*, v. 36, n. 4, p. 57–58, 1983. Disponível em: <http://scitation.aip.org/content/aip/magazine/physicstoday/article/36/4/10.1063/1.2915587>.

MORGAN, H.; GREEN, N. *AC Electrokinetics: Colloids and Nanoparticles*. [S.l.]: Research Studies Press, 2003. (Microtechnologies and microsystems series). ISBN 9780863802553.

NOSÉ, S. A unified formulation of the constant temperature molecular dynamics methods. *The Journal of Chemical Physics*, v. 81, n. 1, p. 511–519, 1984. Disponível em: <http://scitation.aip.org/content/aip/journal/jcp/81/1/10.1063/1.447334>.

NOSÉ, S. Constant temperature molecular dynamics methods. *Progress of Theoretical Physics Supplement*, v. 103, p. 1–46, 1991. Disponível em: <http://ptps.oxfordjournals.org/content/103/1.abstract>.

PALACCI, J. et al. Living crystals of light-activated colloidal surfers. *Science*, American Association for the Advancement of Science, v. 339, n. 6122, p. 936–940, 2013. ISSN 0036-8075. Disponível em: <http://science.sciencemag.org/content/339/6122/936>.

PANKHURST, Q. A. et al. Applications of magnetic nanoparticles in biomedicine. *Journal of Physics D: Applied Physics*, v. 36, n. 13, p. R167, 2003. Disponível em: <http://stacks.iop.org/0022-3727/36/i=13/a=201>.

PASTOR-SATORRAS, R.; RUBÍ, J. M. Particle-cluster aggregation with dipolar interactions. *Phys. Rev. E*, American Physical Society, v. 51, p. 5994–6003, Jun 1995. Disponível em: <http://link.aps.org/doi/10.1103/PhysRevE.51.5994>.

PATNAIK, P. *Handbook of inorganic chemicals*. [S.l.]: McGraw-Hill, 2003. (McGraw-Hill handbooks). ISBN 0-07-049439-8,9780070494398.

PATNAIK, P. R. Noise in bacterial chemotaxis: Sources, analysis, and control. *BioScience*, v. 62, n. 12, p. 1030–1038, 2012. Disponível em: <http://bioscience.oxfordjournals.org/content/62/12/1030.abstract>.

PERRIN, J.; ROUEN, I. chimique de. *Les Atomes*. [S.l.]: F. Alcan, 1913. (Nouvelle collection scientifique).

PORTA, F. et al. Synthesis and full characterisation of nickel(ii) colloidal particles and their transformation into nio. *Colloids and Surfaces A: Physicochemical and Engineering Aspects*, v. 155, n. 2–3, p. 395 – 404, 1999. ISSN 0927-7757. Disponível em: <http://www.sciencedirect.com/science/article/pii/S0927775799000199>.

RAHMAN, A. Correlations in the motion of atoms in liquid argon. *Phys. Rev.*, American Physical Society, v. 136, p. A405–A411, Oct 1964. Disponível em: <http://link.aps.org/doi/10.1103/PhysRev.136.A405>.

RAMASWAMY, S. The mechanics and statistics of active matter. *Annual Review of Condensed Matter Physics*, v. 1, n. 1, p. 323–345, 2010. Disponível em: <http://dx.doi.org/10.1146/annurev-conmatphys-070909-104101>.

RAPAPORT, D. C. *The Art of Molecular Dynamics Simulation*. 2nd. ed. New York, NY, USA: Cambridge University Press, 2004. ISBN 0521825687, 9780521825689.

ROMANCZUK, P. et al. Active brownian particles. *The European Physical Journal Special Topics*, v. 202, n. 1, p. 1–162, 2012. ISSN 1951-6401. Disponível em: <http://dx.doi.org/10.1140/epjst/e2012-01529-y>.

ROMANCZUK, P. et al. Beyond the keller-segel model. *The European Physical Journal Special Topics*, v. 157, n. 1, p. 61–77, 2008. ISSN 1951-6401. Disponível em: <http://dx.doi.org/10.1140/epjst/e2008-00631-1>.

SCHERER, C.; NETO, A. M. F. Ferrofluids: properties and applications. *Brazilian Journal of Physics*, scielo, v. 35, p. 718 – 727, 09 2005. ISSN 0103-9733. Disponível em: <http://www.scielo.br/scielo.php?script=sci_arttext&pid=S0103-97332005000400018&nrm=iso>.

SCHIMANSKY-GEIER, L. et al. Structure formation by active brownian particles. *Physics Letters A*, v. 207, n. 3, p. 140 – 146, 1995. ISSN 0375-9601. Disponível em: <http://www.sciencedirect.com/science/article/pii/037596019500700D>.

SCHMIDLE, H. et al. Phase diagram of two-dimensional systems of dipole-like colloids. *Soft Matter*, The Royal Society of Chemistry, v. 8, p. 1521–1531, 2012. Disponível em: <http://dx.doi.org/10.1039/C1SM06576A>.

SCHMIDLE, H. et al. Two-dimensional colloidal networks induced by a uni-axial external field. *Soft Matter*, The Royal Society of Chemistry, v. 9, p. 2518–2524, 2013. Disponível em: <http://dx.doi.org/10.1039/C2SM27210E>.

SCIAU, P. Nanoparticles in ancient materials: The metallic lustre decorations of medieval ceramics. In: HASHIM, D. A. A. (Ed.). *The Delivery of Nanoparticles*. [S.l.]: InTech, 2012. cap. 25, p. 525–540.

SMOLUCHOWSKI, M. von. Zur kinetischen theorie der brownschen molekularbewegung und der suspensionen. *Annalen der Physik*, WILEY-VCH Verlag, v. 326, n. 14, p. 756–780, 1906. ISSN 1521-3889. Disponível em: <http://dx.doi.org/10.1002/andp.19063261405>.

SNEZHKO, A.; ARANSON, I. S. Magnetic manipulation of self-assembled colloidal asters. *Nat Mater*, Nature Publishing Group, v. 10, n. 9, p. 698–703, Sep 2011. ISSN 1476-1122. Disponível em: <http://dx.doi.org/10.1038/nmat3083>.

SOUSSAN, E. et al. Drug delivery by soft matter: Matrix and vesicular carriers. *Angewandte Chemie International Edition*, WILEY-VCH Verlag, v. 48, n. 2, p. 274–288, 2009. ISSN 1521-3773. Disponível em: <http://dx.doi.org/10.1002/anie.200802453>.

STERN, N. The binac: A case study in the history of technology. *Annals of the History of Computing*, v. 1, n. 1, p. 9–20, Jan 1979. ISSN 0164-1239.

STILLINGER, F. H.; WEBER, T. A. Computer simulation of local order in condensed phases of silicon. *Phys. Rev. B*, American Physical Society, v. 31, p. 5262–5271, Apr 1985. Disponível em: <http://link.aps.org/doi/10.1103/PhysRevB.31.5262>.

SUMPTER, D. et al. Information transfer in moving animal groups. *Theory in Biosciences*, v. 127, n. 2, p. 177–186, 2008. ISSN 1611-7530. Disponível em: <http://dx.doi.org/10.1007/s12064-008-0040-1>.

VELEV, O. D.; GANGWAL, S.; PETSEV, D. N. Particle-localized ac and dc manipulation and electrokinetics. *Annu. Rep. Prog. Chem., Sect. C: Phys. Chem.*, The Royal Society of Chemistry, v. 105, p. 213–246, 2009. Disponível em: <http://dx.doi.org/10.1039/B803015B>.

VERLET, L. Computer "experiments" on classical fluids. i. thermodynamical properties of lennard-jones molecules. *Phys. Rev.*, American Physical Society, v. 159, p. 98–103, Jul 1967. Disponível em: <http://link.aps.org/doi/10.1103/PhysRev.159.98>.

VICSEK, T. et al. Novel type of phase transition in a system of self-driven particles. *Phys. Rev. Lett.*, American Physical Society, v. 75, p. 1226–1229, Aug 1995. Disponível em: <http://link.aps.org/doi/10.1103/PhysRevLett.75.1226>.

WALTHER, A.; MÜLLER, A. H. E. Janus particles: Synthesis, self-assembly, physical properties, and applications. *Chemical Reviews*, v. 113, n. 7, p. 5194–5261, 2013. PMID: 23557169. Disponível em: <http://dx.doi.org/10.1021/cr300089t>.

WATANABE, H.; SUZUKI, M.; ITO, N. Efficient implementations of molecular dynamics simulations for lennard-jones systems. *Progress of Theoretical Physics*, v. 126, n. 2, p. 203–235, 2011. Disponível em: <http://ptp.oxfordjournals.org/content/126/2/203.abstract>.

WIGNER, C. Erklärung des atomistichen Wesens des tropfbar-flüssigen Körperzustandes, und Bestätigung deselben durch die sogenannten Molecularbewengungen. *Annalen der Physik*, v. 118, p. 79–111, 1863.

YABU, H. et al. Hierarchical structures in ab/ac type diblock-copolymer blend particles. *Phys. Chem. Chem. Phys.*, The Royal Society of Chemistry, v. 12, p. 11944–11947, 2010. Disponível em: <http://dx.doi.org/10.1039/C0CP00011F>.

YAN, J.; BAE, S. C.; GRANICK, S. Colloidal superstructures programmed into magnetic janus particles. *Advanced Materials*, v. 27, n. 5, p. 874–879, 2015. ISSN 1521-4095. Disponível em: <http://dx.doi.org/10.1002/adma.201403857>.

YUKAWA, H. On the interaction of elementary particles. *Proc. Phys. Math. Soc. Japan*, v. 17, p. 48–57, 1935.

ZAHN, K.; MÉNDEZ-ALCARAZ, J. M.; MARET, G. Hydrodynamic interactions may enhance the self-diffusion of colloidal particles. *Phys. Rev. Lett.*, American Physical Society, v. 79, p. 175–178, Jul 1997. Disponível em: <http://link.aps.org/doi/10.1103/PhysRevLett.79.175>.